Innate immune signaling and sex differences contribute to neurocognitive impairment, neuroinflammation, and mitochondrial rewiring in a mouse model of Gulf War illness

Joshua D. Bryant[1], Maheedhar Kodali[2], Bing Shuai[2], Saeed S. Menissy[1], Paige J. Graves[1], Ashok K. Shetty[2], Laura Ciaccia West[1*], and A. Phillip West[1*]

[1]Department of Microbial Pathogenesis and Immunology, College of Medicine, Texas A&M University Health Science Center, Bryan, Texas, USA

[2]Institute for Regenerative Medicine, Department of Molecular and Cellular Medicine, College of Medicine, Texas A&M University Health Science Center, College Station, Texas, USA

*Correspondence to: lwest@tamu.edu and awest@tamu.edu

Abstract

Gulf War Illness (GWI) is a chronic, multi-symptom disorder affecting approximately 30 percent of the nearly 700,000 veterans of the 1991 Persian Gulf War. Recent studies have revealed that GWI-related chemical (GWIC) exposure promotes immune activation and metabolic rewiring, which correlate with neurocognitive impairments and other symptoms of GWI. However, the molecular mechanisms and signaling pathways linking GWIC to inflammation, metabolic alterations, and neurological symptoms remain unclear. Mitochondrial dysfunction has been documented in veterans with GWI and rodent models, and because mitochondria are key immune regulators, we hypothesized that alterations to mitochondria-immune crosstalk could contribute to

the development of GWI-related symptoms. Here we show that acute exposure of murine macrophages to GWIC alters mitochondrial respiration and potentiates innate immune signaling and inflammatory cytokine secretion. Using an established mouse model of GWI, we report that neurobehavioral changes, neuroinflammation, and mitochondrial protein rewiring are attenuated in mice lacking the cyclic GMP-AMP synthase (cGAS)-Stimulator of Interferon Genes (STING) and NOD-, LRR- or pyrin domain-containing protein 3 (NLRP3) innate immune pathways. Finally, we report sex differences in response to GWIC, with female mice showing more pronounced cognitive impairment, neuroinflammation, and mitochondrial protein alterations in the brain compared to male mice. Our results provide novel information on sex differences in this model and suggest that STING and NLRP3 are key mediators of the cognitive impairment, inflammation, and mitochondrial dysfunction observed in GWI.

Keywords

Gulf War Illness; Mitochondrial Dysfunction; Innate Immune Signaling; Sex Differences; Memory Impairment; Neuroinflammation

1. Introduction

Gulf War illness (GWI) is a chronic, multi-symptom disorder affecting approximately 25 to 32 percent of the nearly 700,000 veterans of the 1991 Persian Gulf War (PGW-1). Predominantly characterized by brain-related problems including learning and memory deficits, depression, and anxiety, GWI has been linked to synergistic exposure to chemicals including the nerve gas

46 prophylactic pyridostigmine bromide (PB), a reversible acetylcholinesterase inhibitor, and
47 permethrin (Per), an insecticide[1,2].

48 Research over the past few decades has uncovered mechanisms by which exposure to GWI-
49 related chemicals (GWIC) cause GWI pathology and symptoms. Normal function of the brain and
50 nervous system requires significant cellular energy, which is generated within cells by
51 mitochondria. GWIC exposure enhances reactive oxygen species (ROS) production and oxidative
52 stress[3], which may contribute to a vicious cycle of mitochondrial dysfunction (MD) by damaging
53 mitochondrial DNA (mtDNA) and oxidative phosphorylation (OXPHOS) proteins to further
54 augment ROS and trigger progressively increasing mitochondrial stress. Multiple studies have
55 documented MD in both human GWI patients[4,5,6] and in murine models of GWI[3,7,8,9]. Moreover,
56 clinical manifestations of GWI resemble those identified in Chronic Fatigue Syndrome (CFS),
57 which has been linked with MD[5,10].

58 Immune system alterations have also been associated with GWI pathology. Studies of GWI
59 patients have revealed immune changes, including increases in inflammatory cell types[11–13],
60 heightened production of proinflammatory cytokines[11,14–16], and transcriptional profiles that
61 resemble those observed in autoimmune disorders[17]. Parallel immune alterations have also been
62 observed in rodent models of GWI, with increases in proinflammatory cytokines seen in the
63 hippocampi of GWIC-exposed rats[3] and in the brains and serum of GWIC-exposed mice[9,18].
64 However, the role of the innate immune system in GWI pathology, and specifically the
65 identification of signaling cascades responsible for proinflammatory cytokine induction in animal
66 models and Veterans with GWI, remains uncharacterized.

67 Several GWI studies have demonstrated MD and inflammation contemporaneously,
68 suggesting an interaction between these two disease mechanisms[19]. Indeed, in addition to their

69 well-appreciated roles in cellular metabolism and apoptosis, mitochondria are key immune
70 regulators, impacting many aspects of signaling and effector responses in both the innate and
71 adaptive immune system[20]. MD and mtDNA damage can trigger a wide range of inflammatory
72 responses that have been implicated in immune-mediated pathology[21].

73 Based on evidence of MD and inflammation in GWI, and on the documented link between
74 the two, we hypothesized that exposure to GWIC might alter mitochondria-innate immune
75 crosstalk, contributing to inflammatory responses that exacerbate neuropathology and cognitive
76 symptoms of GWI. To test this hypothesis, we employed an established mouse model of GWI in
77 which mice are exposed to the GWIC by intraperitoneal injection for a period of 10 days,
78 developing cognitive impairment and neuroinflammation beginning at 5 months post-exposure[22–
79 24]. In our study, we employed a longitudinal analysis regimen, performing neurocognitive tests at
80 both 5 months and 12 months after acute exposure to GWIC, followed by analysis of mitochondrial
81 protein expression and neuroinflammation in the brain at the terminal timepoint. We used both
82 male and female mice in these experiments to evaluate sex-dependent effects of GWIC, as there is
83 evidence that GWI can be more severe in women[25]. To examine the acute effects of GWIC
84 exposure on metabolism and cell-intrinsic immune responses, we performed a series of *in vitro*
85 experiments using bone marrow-derived macrophages. And finally, we applied this GWIC-
86 exposure model to C57BL/6 genetic knockouts lacking key innate immune sensors that interface
87 with mitochondria and cellular metabolism to evaluate the contributions of these inflammatory
88 signaling pathways to development of GWI pathology. Our results provide important new
89 information on sex differences in GWI-related pathology and reveal that innate immune signaling
90 contributes to neurocognitive impairment, neuroinflammation, and mitochondrial rewiring in a
91 preclinical model of GWI.

92

93

94 **2. Materials and Methods**

95

96 **2.1 Animals, study design, and Gulf War chemical agents**

97 All C57BL/6J wild-type (WT) mice were purchased directly from Jackson Laboratories and
98 allowed to acclimate in the animal facility for 2-4 weeks, or bred in-house. Breeding pairs of NLR
99 Family Pyrin Domain Containing 3 null ($NLRP3^{-/-}$) (JAX strain 021302) and Stimulator of
100 Interferon Genes null ($STING^{gt/gt}$) (JAX strain 017537) mice were purchased from Jackson
101 Laboratories and bred to generate sufficient mice for all experiments. Mice were 8-10 weeks of
102 age upon exposure to GWIC.

103 Briefly, mice were randomly assigned to treatment cohorts: DMSO (vehicle control; 15
104 mice per sex for WT mice, 6 mice per sex for $NLRP3^{-/-}$ and $STING^{gt/gt}$ null mice) or GWIC (15
105 mice per sex for WT, NLPR3 null, and $STING^{gt/gt}$ mice). Mice then underwent an exposure
106 regimen of daily peritoneal injections of 50 microliters of DMSO alone for DMSO cohorts or 50
107 microliters of GWIC (0.7 mg/kg of PB and 200 mg/kg of Per) dissolved in DMSO for GWIC
108 cohorts. Five months after exposure, 6-10 randomly selected mice from DMSO-treated WT and
109 GWIC-treated WT, $NLRP3^{-/-}$, and $STING^{gt/gt}$ cohorts and all DMSO-treated $NLRP3^{-/-}$ and
110 $STING^{gt/gt}$ mice were subjected to neurobehavioral tests as described below. Twelve months after
111 exposure, mice that were behaviorally tested at five months were retested, and then all mice were
112 sacrificed for tissue processing or immunohistochemical analysis.

113 The Animal Care and Use Committee (IACUC) of the Texas A&M University College of
114 Medicine, which ensures compliance with all applicate federal and state regulations for the

115 purchase, transportation, housing, and ethical use of animals for research, has approved all
116 experiments performed in this study. The euthanasia methods employed in the study were
117 consistent with the recommendations of the American Veterinary Medical Association (AVMA).
118 Pyridostigmine bromide (99.9% purity) was purchased from Selleckchem (catalog number
119 HY-B0887) and permethrin (>98% purity) was purchased from MedChemExpress (catalog
120 number S1608).
121
122 **2.2. Behavioral tests for analyses of cognitive and mood function**
123 **2.2.1. Object location test (OLT)**
124 The object location test (OLT) involved three sequential trials (Figure 1A top panel): in the first
125 trial, termed the habituation trial, the mouse was placed at the corner of an empty open field
126 apparatus and allowed to freely explore for five minutes; in the second trial ("sample trial"), which
127 took place twenty minutes after the first trial, the mouse was placed in the corner of the same open
128 field apparatus, which now contained two identical objects placed on opposite sides of the box,
129 and allowed to free explore for five minutes; and in the third, "test" trial, after an inter-trial interval
130 of 20 minutes (5 months post-exposure) or 2 hours (12 months post-exposure), the mouse was
131 placed in the corner of the open field apparatus, with one of the objects remaining in its original
132 location and the other object moved to a novel location. The apparatus was cleaned with 70%
133 ethanol and allowed to air-dry prior to the commencement of each trial. The movement of the
134 mouse in the sample and test trials was continuously video-tracked using the Noldus Ethovision
135 XT program; the nose-point of the mouse coming within 2 cm of an object was recorded by the
136 software as object exploration. Data on time spent exploring both objects, total distance traveled,
137 and velocity of movement during these trials were collected. Percent time spent with the object in

138 a novel location was calculated as total time exploring this object divided by total time exploring
139 both objects. Data in which mice spent less than 10 seconds total exploring both objects in either
140 the sample or test trial were excluded.
141
142 **2.2.2. Pattern separation test (PST)**
143 This test also involved three sequential trials, with a few key changes (Figure 1B, top panel). First,
144 the mouse spent five minutes exploring an empty open field that had a graphic black and white
145 pattern (P1) on the floor of the field and two identical objects. Next, the mouse spent five minutes
146 exploring an empty open field that had a different graphic black and white pattern (P2) on the floor
147 of the field and two different identical objects. Following an inter-trial interval of 3 hours, the
148 mouse spent five minutes in a test trial, in which the P2 pattern was on the floor with one object
149 from the P2 phase (familiar) and one object from the P1 phase (novel). The behavior of the mice
150 was video-tracked as described for the OLT, with data collected on the time exploring the novel
151 and familiar objects, distance traveled, and velocity of movement. Percent time spent with the
152 novel object in P2 was calculated as total time exploring the novel object divided by total time
153 exploring both objects. Data in which mice spent less than 10 seconds total exploring both objects
154 in any trial were excluded.
155
156 **2.2.3. Novel object recognition test (NORT)**
157 This test involved three sequential trials (Figure 1C, top panel): an initial habituation trial as
158 described for the OLT, a second sample trial in which the mouse explored the open field containing
159 two identical objects, and, following an inter-trial interval of 2 hours (5 months post-exposure) or
160 5 hours (12 months post-exposure), a test trial in which one of the original objects was replaced

161 with a novel object placed in the same location The behavior of the mice was video-tracked as
162 described for the OLT, with data collected on the time exploring the novel and familiar objects,
163 distance traveled, and velocity of movement. Percent time spent with the novel object was
164 calculated as total time exploring the novel object divided by total time exploring both objects.
165 Data in which mice spent less than 10 seconds total exploring both objects in either the sample or
166 test trial were excluded.
167

168 **2.2.4. Elevated plus maze (EPMT)**

169 The EPMT uses a grey colored maze consisting of a 60 cm elevated plus-shaped apparatus with
170 four arms, each 35 cm in length and 5 cm in width. Two of the arms are surrounded with walls on
171 three sides of 15 cm in height ("closed arms") and two of the arms are open ("open arms")
172 (Supplementary Figure 2A). Mice were gently placed in the center of the platform, facing a closed
173 arm, and allowed to freely explore the maze for one five minute interval. The movement of the
174 mouse in the sample and test trials were continuously video-tracked using the Noldus Ethovision
175 XT program, with data collected on: the time that the mouse center-point was observed in open
176 arms, closed arms, and the center of the maze; number of visits to open arms, closed arms, and the
177 center of the maze; distance traveled; and velocity of movement.
178

179 **2.3. Immunohistochemical methods**

180 Twelve months after exposure to GWIC, mice were perfused with 4% paraformaldehyde. Brains
181 were postfixed for 18 hours in 4% paraformaldehyde and cryoprotected in 30% sucrose. A cryostat
182 was then used to cut thirty-micrometer thick coronal sections through the entire brain. The sections
183 were collected serially in 24-well plates containing phosphate buffer; sections through the cerebral

184 cortex at hippocampal levels were chosen and processed for immunohistochemical quantification
185 of glial fibrillary acidic protein (GFAP)-positive astrocytes and ionized calcium-binding adaptor
186 molecular 1 (IBA-1)-positive microglia. Briefly, sections were incubated in 20% methanol and 3%
187 hydrogen peroxide in phosphate buffered saline (PBS) for 20 minutes, rinsed three times in PBS,
188 then incubated for 30 minutes in PBS containing 0.1% Triton-X 100 and 10% serum (Sigma).
189 Following this, sections were incubated in primary antibody (rabbit anti-GFAP antibody or goat
190 anti-IBA-1 antibody, both from Abcam) for 18-48 hours, then biotinylated secondary antibody
191 (biotinylated horse anti-goat IgG or biotinylated goat anti-rabbit IgG from Vector Laboratories)
192 for 60 minutes, then an avidin/biotin complex reagent (Vectastain Elite ABC HRP Kit) for 60
193 minutes, with a triple wash in PBS between each incubation step. The peroxidase reaction was
194 developed using Vector SG HRP substrate (Vector Laboratories), then sections were mounted on
195 gelatin-coated slides, dehydrated, cleared, and coverslipped.
196

197 **2.4. Analysis of hippocampal inflammation**

198 Astrocyte hypertrophy was evaluated using ImageJ to calculate area fraction of GFAP+ structures
199 in three regions (CA1, CA3, and dentate gyrus) of the hippocampus in six mice per genotype per
200 sex, for DMSO- and GWIC-exposed cohorts. Multiple sections were imaged per mouse and
201 averaged; image collection and ImageJ analysis were blinded to treatment group. Microglia
202 activation was evaluated by performing morphological analysis. Microglia were identified as IBA-
203 1 structures, while activated microglia were identified as IBA-1+ structures with swollen, ramified
204 cell bodies and short, thick processes[26]. Total microglia and activated microglia were counted for
205 three regions (CA1, CA3, and dentate gyrus, DG) of the hippocampus. Percentages of activated

206 microglia among total microglia were computed and compared. Multiple sections were imaged per
207 mouse and averaged; image collection and morphologic analysis was blinded to treatment group.
208

209 **2.5 Tissue processing and expression analysis**

210 For collection of tissues, animals were sacrificed and brains were quickly removed. The entire
211 hippocampus from both hemispheres and cerebral cortex tissues were micro-dissected from each
212 brain, then snap frozen on dry ice. Cells and tissues were lysed in 1% NP-40 lysis buffer
213 supplemented with protease inhibitor and then centrifuged at 12,000 x g, 4 °C to obtain cellular
214 lysate. After BCA protein assay (Thermo Fisher Scientific), equal amounts of protein (10–20 μg)
215 were separated on 10-20% SDS–PAGE gradient gels, then transferred onto PVDF membranes.
216 After air drying to return to a hydrophobic state, membranes were incubated in primary antibodies
217 (Table 1) at 4°C overnight in 1X PBS containing 1% casein and 0.02% sodium azide. After
218 incubating with HRP-conjugated secondary antibody at room temperature for 1 hour, membranes
219 were developed with Luminata Crescendo Western HRP Substrate (Millipore). Densitometry was
220 performed in ImageJ and normalized to the GAPDH expression level.
221

222 **2.6 In vitro bone marrow-derived macrophage experiments**

223 L929 cells were obtained from ATCC and maintained in DMEM (D5796) (Sigma) supplemented
224 with 10% FBS (97068-085) (VWR). Bone marrow-derived macrophages (BMDMs) were
225 generated from bone marrow collected from femurs and tibiae isolated from male and female mice.
226 Briefly, legs were dissected from mice and muscle and tissue were removed. Bones were immersed
227 in 70% EtOH then washed with PBS. Bones were crushed with a mortar and pestle and the marrow
228 was collected in DMEM. The marrow was passed through a 70 μm mesh strainer, then blood cells

229 were lysed using ACK lysis buffer. Remaining cells were passed through a 40 μm mesh strainer
230 and plated on Petri dishes in DMEM containing 10% FBS and 30% L929 culture media for 7 days.
231 For all experiments, BMDMs were plated at a density of 6 x 10^5 cells/mL unless otherwise
232 indicated. After cells were plated and allowed to adhere for 2-3 hours, cells in GWIC treatment
233 group were treated overnight with permethrin (10 μM final) and/or pyridostigmine bromide (PB,
234 100 ng/mL) as indicated. LPS treatment was done with LPS-B5 Ultrapure (InvivoGen) at a
235 concentration of 200 ng/mL unless otherwise indicated. Transfection of HSV-60bp interferon-
236 stimulatory DNA (ISD) (InvivoGen) into the cytosol of BMDMs was performed using
237 Polyethyleneimine (PEI) (43896) (Alfa Aesar).
238
239 **2.7 ELISA**
240 Primary, secondary, and detection antibodies were purchased from BioLegend. Detached cells and
241 debris were removed from cell culture supernatant by centrifugation prior to the assay. After
242 incubating half-well ELISA plates in capture antibodies at 4°C overnight, plates were blocked with
243 PBS containing 10% FBS at room temperature for 1 hour. Cell culture supernatants were diluted
244 80-240x (for IL-6) or 2-20x (for TNF-α) in blocking buffer. Standards and cell culture supernatant
245 were added to the ELISA plates and incubated at room temperature for 2 hours. Plates were
246 incubated at room temperature with biotin-conjugated secondary antibody for 1 hour, followed by
247 Avidin-HPR and detection with a TMB Substrate Set (BioLegend). Plates were washed 4 times
248 with PBS containing 0.05% Tween-20 between each step.
249
250 **2.8 Metabolic analysis**

251 The Seahorse XFe96 Analyzer was used to measure mitochondrial respiration and glycolysis
252 simultaneously following a modified protocol. Briefly, BMDMs were plated at a density of $6x10^4$
253 cells/well in 80µL of culture medium in an Agilent Seahorse XF96 Cell Culture Microplate. After
254 3 hours, an additional 80 µL of medium was added containing permethrin (10 µM final) and/or
255 pyridostigmine bromide (100 ng/mL final) as indicated. After incubating overnight, an additional
256 40 µL culture medium containing LPS (200 ng/µL final) was added as indicated. Following a 6 hr
257 incubation, cells were washed and media was replaced with XF assay medium (Base Medium
258 Minimal DMEM lacking glucose, glutamine, and bicarbonate, supplemented with 2 mM Ala-Gln,
259 pH 7.4) prior to analysis. Oxygen consumption rate (OCR) and extracellular acidification rate
260 (ECAR) were measured after sequential addition of glucose 25 mM; oligomycin (1.5 uM); FCCP
261 (1.5 µM) + sodium pyruvate (1mM) and; antimycin A (833 nM) + rotenone (833 nM). Beginning
262 the run with glucose omitted from the medium allows both respirator and glycolytic parameters to
263 be determined in the same run. Respiratory and glycolytic parameters were calculated using the
264 equations outlined in the Seahorse XF Mito Stress Test and Glycolysis Stress Test manuals.
265
266 **2.9 Statistical analyses**
267 All p-values were calculated using two-tailed, unpaired, Student's t-test, one-way ANOVA with
268 Tukey's multiple comparison, or the two-stage step-up method to yield q values that have been
269 corrected for the false discovery rate in Excel or GraphPad Prism as indicated in figure legends.
270
271
272 **3. Results**
273

274 **3.1. Female GWIC-exposed mice display more pronounced impairments in cognitive**
275 **function and mood than male GWIC-exposed mice.**

276 To establish GWIC-dependent cognitive symptoms in our model, we employed a battery of tests
277 to characterize neurobehavioral changes following GWIC exposure. A randomly selected subset
278 of GWIC- and DMSO-treated male and female C57BL/6 wild-type (WT) mice were tested for the
279 hippocampal-dependent ability to perceive changes in the environment using an object location
280 test (OLT)[27]. Notably, at both 5 months and 12 months post-exposure, female GWIC-exposed mice
281 showed impairment, failing to show a statistically significant affinity for the object in a novel
282 location during the testing phase (Fig 1A). Male GWIC-exposed mice did not display this
283 impairment, nor did DMSO-exposed mice, regardless of sex. The same cohorts were tested for
284 pattern separation ability using the pattern separation test (PST), which relies on the integrity of
285 the dentate gyrus of the hippocampus[27]. As observed in the OLT, female GWIC-exposed mice
286 showed impairment in the testing phase, while male GWIC-exposed mice and DMSO-exposed
287 mice of both sexes showed a statistically significant increase in affinity for the novel object in
288 pattern 2, reflecting pattern separation ability (Fig 1B). For both tests, control data for total
289 exploration time, total distance moved, and velocity of movement in the testing phase were similar
290 (Supplemental Figure 1), indicating that variable object exploration or motor deficits do not
291 explain the differences in test performance. Rather, these results indicate an impairment in
292 hippocampal function in female, but not male, GWIC-exposed mice at 5 and 12 months post-
293 exposure.

294 We observed similar sex-differences in tests of mood function following GWIC-exposure.
295 At 5 months post-exposure, we used the elevated plus maze test (EPMT) (Supplemental Figure
296 2A) to determine unconditioned response to a potentially dangerous environment and anxiety-

297 related behavior[28,29]. We observed a trend in which female, not male, GWIC-exposed mice spent
298 less time in open maze arms (Supplementary Figure 2B) and more time in closed maze arms or
299 the center (Supplemental Figure 2D), consistent with anxiety-related behaviors. Calculation of the
300 ratio of visits to the closed arms or center region of the maze versus visits to the open arms revealed
301 a statistically significant increase in preference for the closed arms or center of the maze in GWIC-
302 exposed female mice, but not GWIC-exposed male mice, as compared to DMSO-exposed
303 counterparts (Supplemental Figure 2C). As with the OLT and PST, control data were similar
304 among all cohorts (Supplemental Figure 2E), ruling out motor deficits as the underlying reason for
305 differences in EPMT performance. These results suggest that an increase in anxiety-related
306 behavior is an additional sex-dependent neurobehavioral change following GWIC-exposure.
307

308 **3.2. Female and male GWIC-exposed mice display similarly impaired object recognition**
309 **memory.**

310 Cohorts of mice also were tested for object recognition memory using the novel object recognition
311 test (NORT). Both male and female GWIC-exposed mice failed to show an affinity for the novel
312 object during the testing phase of the NORT, indicating impaired recognition memory. DMSO-
313 exposed mice, regardless of sex, spent a significantly greater amount of object exploration time
314 with the novel object during the testing phase (Figure 1C). As with the OLT and PST tests, control
315 data were comparable among groups, (Supplemental Figure 1), indicating that variable object
316 exploration or motor deficits do not explain the differences in test performance.

317 While both male and female GWIC-exposed mice display impairment on the NORT, which
318 depends primarily upon the integrity of the perirhinal cortex region of the cerebral cortex and
319 partially the hippocampus[27], only female GWIC-exposed mice display impairment on two tests

320 (OLT, PST) that rely on hippocampal function. This suggests that female GWIC-exposed mice
321 may exhibit increased hippocampal pathology, which may include mitochondrial alterations and
322 neuroinflammation, compared to GWIC-exposed male mice.
323
324 **3.3. GWIC-exposed mice display sex-dependent alterations in expression of mitochondrial**
325 **proteins in the hippocampus and cerebral cortex.**
326 To evaluate mitochondrial changes in the brains of these male and female GWIC-exposed mice,
327 we performed comparative expression analysis of regions required for performance of these
328 neurocognitive tests: the hippocampus, required for the OLT, NORT, and PST, and the cerebral
329 cortex, required for the NORT. Following completion of behavioral tests at 12 months, brains were
330 microdissected to isolate the hippocampus and cerebral cortex (CC), and protein extracts generated
331 were subjected to Western blotting and densitometry quantification.
332 Examination of an array of mitochondrial proteins revealed widespread rewiring of
333 mitochondrial protein expression, particularly enzymes involved in oxidative phosphorylation
334 complexes I-V (OXPHOS CI-CV). Interestingly, the directionality of the expression changes
335 varied between male and female mice, with the expression of several OXPHOS proteins
336 (NDUFB8, UQCRC2, and MT-COI) significantly increasing in the hippocampi of GWIC-exposed
337 female mice (Figure 2A) but trending towards a decrease in the hippocampi of GWIC-exposed
338 male mice (Figure 2B). Similarly, moderate reductions in abundance of MnSOD (mitochondrial
339 superoxide dismutase that generates hydrogen peroxide), OGDH (TCA cycle enzyme), and TFAM
340 (mtDNA packaging protein) were observed in female, but not male, GWIC-exposed hippocampi.
341 Notably, this observation of more pronounced changes in mitochondrial expression within the

342 hippocampus of female GWIC-exposed mice parallels our earlier finding that GWIC-exposed
343 female mice show greater impairment in hippocampal-dependent neurocognitive tests.
344 Analysis of extracts from the CC also reveals sex-dependent directionality of expression
345 changes. Although expression of UQCRC2 was largely unchanged in the hippocampi of GWIC-
346 exposed male mice, it is significantly decreased in CC extracts from these animals (Figure 2D). In
347 contrast, UQCRC2 levels in CC extracts isolated from female GWIC-exposed mice show a modest
348 increase (Figure 2C), echoing the varied directionality observed in the hippocampus. Similarly,
349 we observed a trending decrease in expression of MT-COI, ATP5A, and SDHA in CC extracts of
350 male, but not female, mice. Overall, these changes in mitochondrial protein abundance reveal sex-
351 dependent OXPHOS remodeling, which persists for 12 months after exposure to GWIC and tracks
352 with neurocognitive impairments.
353
354 **3.4. Female GWIC-exposed mice exhibit increased neuroinflammation as compared to male**
355 **GWIC-exposed mice.**
356 To assess neuroinflammation after GWIC exposure, perfused brains from female and male mice
357 were fixed, sectioned, and processed for immunohistochemical quantification of glial fibrillary
358 acidic protein (GFAP)-positive astrocytes and ionized calcium-binding adaptor molecular 1 (IBA-
359 1)-positive microglia. Quantification of astrocytes in the dentate gyrus (DG), CA1, and CA3
360 regions of the hippocampus (Figure 3) revealed that female GWIC-exposed mice displayed
361 significantly increased GFAP+ structures in all three hippocampal regions as compared to female
362 DMSO-exposed mice. Male GWIC-exposed mice show significantly increased GFAP+ structures
363 in the DG region and CA3 region only. This observation, which indicates more widespread
364 hippocampal inflammation in female GWIC-exposed mice as compared to male GWIC-exposed

365 mice, is consistent with our findings that female GWIC-exposed mice display increased
366 impairment on hippocampal-dependent neurobehavioral tests.

367 A study by Zakirova and colleagues of neuroinflammation in this murine model of GWIC-
368 exposure have likewise observed significant increases of astrocyte hypertrophy in the dentate
369 gyrus of the hippocampus, as measured by GFAP quantification. Notably, this study, which
370 exclusively used male mice, did not observe a significant increase in activated IBA-1+ microglia
371 following GWIC-exposure[24]. In contrast, when we performed blinded morphological scoring of
372 IBA-1+ cells with the DG, CA1, and CA3 of hippocampi from GWIC- and DMSO-exposed male
373 and female mice, we observed a significant increase in activated microglia within the DG of
374 female, but not male, GWIC-exposed mice as compared to DMSO-exposed mice (Supplementary
375 Figure 7A). Significant increases were not observed in the CA1 or CA3 hippocampal regions of
376 female or male GWIC-exposed mice, and male GWIC-exposed mice displayed a significant
377 reduction in IBA-1+ cells with an activated morphology within the CA1 region, consistent with
378 decreases in percent fraction of IBA-1+ cells observed by Zakirova *et al*. Our findings therefore
379 suggest a novel sex-dependent increase in activated microglia within the DG region of the
380 hippocampus in this model of GWIC-exposure.

381

382 **3.5. GWIC-exposure of cells results in metabolic alterations, enhanced expression of**
383 **interferon-stimulated genes, and increased production of inflammatory cytokines.**

384 Our findings are consistent with the notion that GWIC exposure causes lasting mitochondrial
385 rewiring and neuroinflammation. However, a direct effect of GWIC on metabolism and/or innate
386 immune signaling has not been documented. Therefore, to characterize the immediate impact of
387 GWIC on mitochondrial function and cell-intrinsic innate immune responses, we performed a

388 series of acute, in vitro experiments using bone marrow-derived macrophages (BMDMs). While
389 not derived from the brain, BMDMs provide a robust cellular platform to evaluate mitochondrial
390 function, innate immune responses, and the dynamic interplay between these pathways[30]. To first
391 evaluate GWIC-dependent changes in oxygen consumption and glycolysis, BMDMs were treated
392 overnight with permethrin (Per) alone, pyridostigmine bromide (PB) alone, or, as in *in vivo*
393 experiments, both of these GWIC (Per-PB), then subjected to analysis of mitochondrial respiration
394 using a Seahorse XF96 Analyzer. Per or Per-PB exposed BMDMs exhibited significantly
395 increased basal mitochondrial oxygen consumption (OCR), with unchanged maximal respiration
396 (Figure 4A), while treatment with PB only failed to increase basal respiration and resulted in
397 significantly diminished maximal respiration. Treatment with Per, PB, or Per-PB decreased spare
398 respiratory capacity, accompanied by an increase in proton leak for Per- and Per-PB-treated
399 BMDMs. Overall, these data indicate that acute exposure to GWIC induces changes to
400 mitochondrial OXPHOS and are consistent with the in vivo findings described in Section 3.3.
401 Additional changes were observed when BMDMs were treated with bacterial lipopolysaccharide
402 (LPS, an agonist of the innate immune sensor Toll-like receptor 4 (TLR4)) in combination with
403 GWIC. Per or Per-PB pretreatment followed by LPS resulted in an increase in basal respiration,
404 as seen in mock-treated cells, as well as a significant increase in maximal respiration (Figure 4B).
405 Interestingly, LPS treatment resulted in significantly increased spare respiratory capacity upon
406 exposure to all three GWIC combinations, though this could be due to the increase in maximal
407 respiration. Following LPS treatment, proton leak was increased only in Per cells. Additional
408 studies analyzing a surrogate marker of glycolysis, the extracellular acidification rate (ECAR),
409 revealed that while glycolysis was largely unchanged following GWIC-exposure alone
410 (Supplementary Figure 3B), treatment with GWIC plus LPS resulted in cells becoming more

411 glycolytic (Supplementary Figure 3C), consistent with the immunometabolic changes typically
412 seen in inflammatory M1 macrophages.

413 Prior work has shown that systemic LPS-induced TLR4 activation contributes to GWIC-
414 related neuroinflammation[31]. To examine the direct effects of GWIC exposure on innate immune
415 signaling, we first measured expression of induced proteins following LPS-stimulation of BMDMs
416 that had been pre-treated with Per, PB, or Per-PB. We observed modest increases in expression of
417 the interferon regulatory factor IRF1 in BMDMs exposed to LPS plus Per and/or Per-PB, as well
418 as modestly elevated levels of the interferon stimulated gene (ISG) IFIT3 after 6 hours of LPS plus
419 PB and Per-PB exposure (Supplementary Figure 3A). Additional work in BMDMs revealed
420 synergy between the STING innate immune pathway, as transfection of interferon stimulatory
421 DNA (ISD) to activate STING after pretreatment with GWIC resulted in modestly elevated ISG
422 expression (Figure 4C). Moreover, we noted an increase in pro-IL-1β cytokine abundance after
423 LPS plus GWIC (Figure 4D). In fact, PB increased Caspase I cleavage to the active p20 isoform
424 in both untreated and LPS-treated cells, a process that requires activation of cytosolic
425 inflammasomes such as NLRP3. Finally, ELISA analysis of BMDMs revealed that GWIC
426 exposure synergized with LPS stimulation and resulted in increased proinflammatory cytokine
427 production: Per or Per-PB treatment led to increased production of both IL-6 and TNF-α after 24
428 hours of LPS treatment (Figure 4E). Interestingly, though PB alone inhibited IL-6 and TNF-α
429 production, it acted synergistically with Per and enhanced IL-6 and TNF-α production over Per
430 treatment alone. Overall, our results reveal that GWIC induce immunometabolic rewiring of
431 OXPHOS and glycolysis in BMDMs and potentiate inflammatory responses to innate immune
432 stimulation.
433

434 **3.6. Ablation of STING or NLRP3 signaling improves neurocognitive deficits and**
435 **neuroinflammation and blunts changes in mitochondrial protein expression following**
436 **GWIC-exposure.**

437 Our in vivo experiments using a mouse model of GWI have demonstrated neurocognitive deficits,
438 changes in expression of mitochondrial proteins, and hippocampal inflammation caused by GWIC,
439 with more severe symptoms observed in female mice. Our *in vitro* experiments using BMDMs
440 revealed metabolic changes and heightened innate immune responses following GWIC treatment,
441 including increased production of ISGs and the proinflammatory cytokines IL-1β, IL-6, and TNFα.
442 Notably, BMDM experiments suggested potentiated TLR4, STING, and NLRP3 innate immune
443 signaling in response to acute GWIC exposure.

444 Stress, infection, or injury can cause MD, which leads to the release of mitochondrial
445 constituents such as mtDNA, mitochondrial lipids (cardiolipin), *N*-formyl peptides, mitochondrial
446 metabolites (succinate), and high concentrations of ATP[21]. These so-called damage-associated
447 molecular patterns (DAMPs) then trigger the innate immune system via several paths. mtDNA can
448 be detected by the enzyme cGAS, which then generates the cyclic dinucleotide cGAMP, a second
449 messenger that binds and activates STING[32] for expression of type I interferons and ISGs[33].
450 Likewise, over-production of ROS, mtDAMP release, and altered mitochondrial dynamics due to
451 MD engage the NLRP3 inflammasome, triggering processing of pro-interleukin-1 beta (pro-IL-
452 1β) into IL-1β[34,35]. Both STING and NLRP3 are therefore key mechanisms by which MD and
453 mtDAMPs can engage the innate immune system, and the increases in ISGs and IL-1β observed
454 in Figure 4 and Supplementary Figure 3 implicate both pathways downstream of GWIC.

455 To interrogate the contribution of STING and NLRP3 signaling to neurobehavioral
456 changes, neuroinflammation, and mitochondrial rewiring following GWIC exposure, cohorts of

457 STING$^{gt/gt}$ and NLRP3$^{-/-}$ mice on a C57BL/6 background were exposed to DMSO or GWIC in
458 parallel to wild-type C57BL/6 (WT) mice. STING$^{gt/gt}$ mice are homozygous for an I199N missense
459 mutant allele in the *Sting* gene and express no STING protein[36], while NLRP3$^{-/-}$ mice are
460 homozygous for a neo cassette in the coding region of *Nlrp3* and are therefore deficient in the
461 NLRP3 inflammasome[37].

462 Neurobehavioral tests of STING$^{gt/gt}$ mice revealed that observed impairments of GWIC-
463 exposed mice are STING-dependent. In contrast to WT GWIC-exposed cohorts, GWIC-treated
464 STING$^{gt/gt}$ female mice demonstrated rescue of object location memory by successfully
465 completing the OLT at both 5 months post-exposure (Figure 6A) and at 12 months post-exposure
466 (Supplementary Figure 4A). Similarly, GWIC-treated STING$^{gt/gt}$ female mice at 5 months post-
467 exposure (Figure 6A) and GWIC-treated STING$^{gt/gt}$ male mice at 12 months post-exposure
468 (Supplementary Figure 5B) were unimpaired in the NORT. These findings suggest that STING
469 signaling may contribute to impairment of both hippocampal function in female mice and cerebral
470 cortex function in male and female mice following GWIC exposure.

471 Interestingly, neurobehavioral tests of NLRP3$^{-/-}$ mice suggest that neurobehavioral changes
472 due to GWIC exposure are only partially NLRP3-dependent. Like GWIC-treated female WT mice,
473 NLRP3$^{-/-}$ mice display impaired object location recognition at 5 months (Figure 7A) and 12 months
474 (Supplementary Figure 5) post-exposure, indicating that NLRP3 signaling is not important for the
475 development of this neurocognitive change. Additionally, although NLRP3$^{-/-}$ female mice at 5
476 months post-exposure show restored novel object recognition (Figure 7A), this restoration was lost
477 at 12 months post-exposure (Supplementary Figure 4B).

478 Ablation of STING signaling and the NLRP3 inflammasome appears to improve mood
479 function in female mice following GWIC-exposure. While WT GWIC-exposed female mice

480 displayed a statistically significant preference for the closed arms or center of the maze during the
481 EPMT, STING$^{gt/gt}$ and NLRP3$^{-/-}$ female mice fail to show this preference (Supplementary Figure
482 4D). STING$^{gt/gt}$ and NLRP3$^{-/-}$ GWIC-exposed male mice behave similarly to WT counterparts,
483 without an observed preference.

484 The results of the experiments described above demonstrate that STING and NLRP3
485 contribute to GWI-dependent neurocognitive changes to a varying degree. Additional
486 neurobehavioral tests were more difficult to interpret at the inter-trial intervals employed in the
487 study. For example, both DMSO- and GWIC-treated STING$^{gt/gt}$ female mice are deficient in novel
488 object recognition at 12 months post-exposure, indicating non-treatment specific, aging-related
489 neurobehavioral changes in these mice (Supplementary Figure 4B). Similarly, STING$^{gt/gt}$ and
490 NLRP3$^{-/-}$ female and male mice showed impaired pattern separation ability, regardless of
491 treatment, at 5 months post-exposure (Supplementary Figure 4C). Because of this, we cannot draw
492 conclusions from 12 month post-exposure NORT tests in female mice or 5 month post-exposure
493 PST tests in female or male mice. While STING signaling or the NLRP3 inflammasome may in
494 fact impact neurobehavioral changes as measured by these assays, changes to the DMSO-treatment
495 control mice make conclusions impossible.

496 Other tests were also inconclusive. GWIC-treated STING$^{gt/gt}$ male mice at 5 months and
497 NLRP3$^{-/-}$ male mice at 5 and 12 months post-exposure successfully completed the NORT.
498 However, the validity of this data is uncertain due to the failure of DMSO-treated control cohorts
499 to spend significantly increased time with the novel object (Supplementary Figure 5). In the case
500 of the DMSO-treated STING$^{gt/gt}$ mice at 5 months post-exposure, controls measurements indicated
501 decreased movement and object exploration (Supplemental Figure 5). However, for all other

502 groups and tests, control data indicate that variable object exploration or motor deficits do not
503 explain test performance (Supplementary Figure 5).

504 In the WT GWIC-exposed female mice, deficiencies in neurobehavioral tests correlated
505 with increased astrocyte hypertrophy in three regions of the hippocampus. In contrast, both
506 STING$^{gt/gt}$ and NLRP3$^{-/-}$ female mice failed to show increased astrocyte hypertrophy in the DG
507 (Figure 6B) or the CA1 and CA3 regions (Supplementary Figure 6A, B) as compared to DMSO-
508 treated WT controls. Expression of GFAP in the hippocampi of DMSO-treated WT, STING$^{gt/gt}$,
509 and NLRP3$^{-/-}$ were comparable (Supplementary Figure 6C), suggesting that this observation is due
510 to lessened GWIC-induced neuroinflammation in the absence of STING or NLRP3. In addition,
511 analysis of IBA-1+ cells within the hippocampus also revealed a decrease in activated microglia
512 within the DG of STING$^{gt/gt}$, and NLRP3$^{-/-}$ GWIC-exposed female mice (Supplementary Figure
513 7) as compared to WT GWIC-exposed female mice.

514 STING and NLRP3 therefore play a role in driving neurocognitive changes and
515 neuroinflammation following GWIC exposure. To assess the impact on mitochondrial expression
516 changes, extracts of the hippocampi and cerebral cortices of DMSO- and GWIC-exposed
517 STING$^{gt/gt}$ and NLRP3$^{-/-}$ mice were analyzed as in Figure 2. Hippocampal extracts from both
518 STING$^{gt/gt}$ and NLRP3$^{-/-}$ female mice no longer show the significant increase in NDUFB8 observed
519 in WT female mice, and STING$^{gt/gt}$ female mice also show a downward trend in UQCRC2
520 expression and a significant decrease in MT-COI, in contrast to the significant upregulation of
521 both in WT female mice. We also observed an upward trend of expression for UQCRC2, MT-COI,
522 ATP5A, and SDHA in the CC of STING$^{gt/gt}$ males, which were all downregulated in WT males.
523 Overall, expression analysis of STING$^{gt/gt}$ and NLRP3$^{-/-}$ brains echoes other findings with these
524 mice: the absence of these signaling hubs reduces cognitive impairment, neuroinflammation, and

525 mitochondrial expression changes, with findings indicating a more significant role for STING than
526 for NLRP3.
527
528
529 **4. Discussion**
530
531 Using an established murine model of GWI[22,29,24], we demonstrated that GWIC-exposed female
532 mice display impaired object location memory and novel object recognition at 5 and 12 months
533 post-exposure, and impaired pattern separation at 5 months post-exposure. These results show that
534 female mice have more severe GWIC-dependent neurocognitive impairment than males, which in
535 our studies showed impairment only in novel object recognition and no anxiety-related behavior
536 as measured by the EPMT. A previous study examining both female and male C57BL/6 mice also
537 demonstrated increased anxiety in female mice, as measured by the open field test (OFT)[38].
538 However, the majority of GWI rodent model studies have used male mice only, using tests
539 including the Barnes maze[24,29,7,39] , forced swim test[39,40], and OFT[38,35,26] to reveal cognitive
540 impairment, fatigue, and anxiety-related behavior. We tested both female and male GWIC-
541 exposed mice using the OLT, NORT, and PST, which has been used in GWI rat models to show
542 impairment in male animals with demonstrated hippocampal inflammation[27,42,43,44]. We also used
543 the EPMT, which has shown disinhibition type behaviors in GWIC-exposed male mice[29] that we
544 did not observe, likely due to differences in time post-exposure. This study is therefore the first
545 time female GWIC-exposed mice have been evaluated for neurocognitive impairment using this
546 battery of tests. While women represented a relatively small percentage (7%) of the active duty
547 population during PGW-1[45], chronic GWI conditions differ in female and male PGW-1 veterans[46],

548 with some studies showing female veterans PGW-1 as more likely to meet the clinical criteria of
549 GWI and to display heightened, longer-lasting GWI symptoms than male veterans[47,48]. Therefore,
550 there is a critical need to better understand sex differences in GWI pathology. The more significant
551 neurocognitive impairment that we observed in female mice makes a strong argument for inclusion
552 of both sexes in future pre-clinical GWI studies involving rodents.

553 In addition to cognitive impairment, we observed astrocyte hypertrophy within all three
554 examined regions (dentate gyrus, CA1, and CA3) of the hippocampi of GWIC-exposed female
555 mice, as compared to only two regions (DG and CA3) in male mice. Comparison of DMSO-
556 exposed female and male mice revealed that control males appear to have heightened astrocyte
557 hypertrophy as compared to control females, which may explain the diminished GWIC-dependent
558 increase. We also observed an increase in IBA-1+ microglia with an activated morphology in the
559 dentate gyri of GWIC-exposed female mice, with a decrease observed in GWIC-exposed male
560 mice, consistent with a previous study[29]. Overall, this novel observation of more severe
561 hippocampal inflammation observed in GWIC-exposed female mice further emphasizes the value
562 of using both male and female mice for future GWI study.

563 Our analysis of expression of mitochondrial proteins in the hippocampi of GWIC-exposed
564 mice adds to the growing body of evidence that MD is an important factor in the pathology of
565 GWI. MD[49] and mtDNA lesions[50] have been documented in GWI patients, and animal studies
566 analyzing expression of nuclear and mitochondrially encoded OXPHOS proteins from whole brain
567 extracts have demonstrated widespread expression changes in mice[51] and rats[3]. We observed
568 decreases in OXPHOS proteins in male mice exposed to GWICs in both the hippocampus and
569 peripheral cortex. In contrast, OXPHOS protein expression in female mice increased in response
570 to GWICs, particularly in the hippocampus, while other mitochondrial proteins including SDHB,

571 MnSOD, TFAM, and OGDH show a modest decrease in expression. This suggests a general
572 rewiring of mitochondrial protein expression, rather than a wholesale decrease in all mitochondrial
573 proteins, that is most severe in hippocampi of female mice.

574 *In vitro* studies centered around acute treatment of BMDMs provided further evidence of
575 disruptions to mitochondrial metabolism. Of the two GWIC, permethrin was the main driver for
576 alterations to mitochondrial respiration, leading to an increase in basal respiration, loss of spare
577 respiratory capacity, and increase in proton leak. Though PB alone had little effect, it appeared to
578 act synergistically with Per, causing further alterations to basal respiration and spare respiratory
579 capacity in control cells and an increase in spare respiratory capacity in LPS-treated cells. We
580 observed a similar synergistic interaction when we analyzed production of IL-6 and TNFα after
581 LPS stimulation. Per alone induced an increase in cytokine release, while PB alone had little effect;
582 however, treatment with Per and PB together induced an even stronger response. A likely
583 explanation for this observation is that Per and PB are acting through separate but complimentary
584 pathways. BMDMs treated with Per showed increased expression of ISGs than either untreated or
585 PB treated cells after induction with LPS or ISD. Alternatively, BMDMs treated with PB displayed
586 increased expression of pro-IL-1β and increased cleavage of Caspase I. Thought the effect was
587 subtle, this suggests low levels of activation of the NLRP3 inflammasome in response to PB.
588 Consistent with this notion, elevated serum levels of IL-1β and IL-6 have been observed in patients
589 with GWI, and elevated IL-1β, IL-6, and TNFα have been observed in the brains of mice exposed
590 to GWICs[3,43,52–54].

591 As in other studies, our analysis of C57BL/6 WT GWIC-exposed mice and of GWIC-
592 treated BMDMs demonstrated contemporaneous MD and inflammation. GWIC-exposure
593 experiments with STING$^{gt/gt}$ and NLRP3$^{-/-}$ mice suggest a link between the two. Loss of STING in

594 female mice restores hippocampal-dependent object location memory at both 5 and 12 months
595 post GWIC exposure and novel object recognition ability at 5 months post-exposure; loss of
596 STING also restores novel object recognition in male GWIC-exposed mice. These data strongly
597 suggest a role for STING in driving neurocognitive changes following GWIC-exposure. Loss of
598 NLRP3 has a subtler effect, restoring novel object recognition in female GWIC-exposed mice at
599 5 months, but not 12 months, post-exposure. This may indicate a role for NLRP3 in relatively
600 short-term impairment in novel object recognition following GWIC-exposure. These findings are
601 limited by the behavioral tests we employed and by the validity of these tests. As described in
602 Section 3.6, several of the tests of $STING^{gt/gt}$ and $NLRP3^{-/-}$ mice were inconclusive due to
603 impairment observed in control animals or by the failure of cohorts to spend sufficient time in
604 object exploration. However, we were able to draw conclusions from several OLT, NORT, and
605 EPMT tests, which on their own suggest a significant role for STING and a potentially lesser,
606 time-dependent role for NLRP3 in driving neurocognitive impairment.

607 Analysis of neuroinflammation and expression of mitochondrial proteins within the
608 hippocampi and cerebral cortices of GWIC-exposed mice also support a role for STING and
609 NLRP3 in GWI. Loss of STING or NLRP3 in female mice results in a significant diminishment
610 of astrocyte hypertrophy in all three regions of the hippocampus as compared to GWIC-exposed
611 WT females, as well as a significant decrease in microgliosis within the DG. The rewiring of
612 mitochondrial expression due to GWIC-exposure is also blunted or reversed in $STING^{gt/gt}$ and
613 $NLRP3^{-/-}$ mice. STING and NLRP3 therefore join TLR4[31] as innate immune sensors linked to
614 GWI-related pathology in murine models. Remaining questions include in which cell types and
615 tissues STING and/or NLRP3 signaling occurs to influence GWI symptoms, as well as the timing
616 of signaling following GWIC exposure. Future study using conditional transgenic models will

617 need to be conducted to address these questions. Comprehensive assessment of these innate
618 immune pathways in patient samples is also needed to confirm whether our findings extend to
619 veterans with GWI. If indeed these pathways are active, targeted intervention using STING and
620 NLRP3 inhibitors may be effective at alleviating some GWI symptoms and improving the
621 healthspan of this population.

622 Finally, therapeutic targeting of mitochondria to directly improve metabolic function is a
623 viable treatment strategy for GWI. Indeed, veterans with GWI have shown improvements in
624 symptoms in response to Coenzyme Q10 [55], an antioxidant and OXPHOS electron carrier known
625 to have beneficial effects on mitochondria, or KPAX002, a combination treatment designed to
626 boost mitochondrial function[56]. Emerging links between mitochondria and the innate immune
627 system raise the possibility that therapeutic approaches to improve mitochondrial health may also
628 serve to decrease inflammation, likely by reducing mtDAMP release/accumulation. Our work
629 implicates two of the main mtDAMP sensing pathways, STING and NLRP3, to GWIC-related
630 inflammation, mitochondrial/metabolic rewiring, and cognitive deficits. Therefore, an intriguing
631 future direction is to evaluate how different mitochondrial therapeutics affect neurocognitive
632 impairment, neuroinflammation, and mitochondrial protein expression within the brain of GWIC-
633 exposed mice to understand the efficacy, mechanisms, and perhaps sex-specific effects, of these
634 treatments.

635

636 **Acknowledgements**

637 We thank Sahithi Attaluri for assistance with immunohistochemical analysis and Dr. Alexandra
638 Trott, Associate Director of the TAMU Rodent Preclinical Phenotyping Core, for assistance with
639 behavioral tests. This work was supported, in part, by a grant from NIEHS P30 ESES029067 and

640 by awards W81XWH-17-1-0446 (to A.P.W.), W81XWH-16-1-0480 (to A.K.S.), and W81XWH-
641 17-1-0447 (to A.K.S.) from the Office of the Assistant Secretary of Defense for Health Affairs
642 through the Peer Reviewed Medical Research Programs, Gulf War Illness Research Program.
643 Opinions, interpretations, conclusions, and recommendations are those of the authors and are not
644 necessarily endorsed by the Department of Defense or the United States Government.
645

646 **Competing interests statement**

647 The authors declare no competing interests.

648

Figure 1. Exposure of C57BL/6 wild-type mice to GWIC results in sex-dependent impairment in spatial memory, pattern separation, and novel object reocognition.

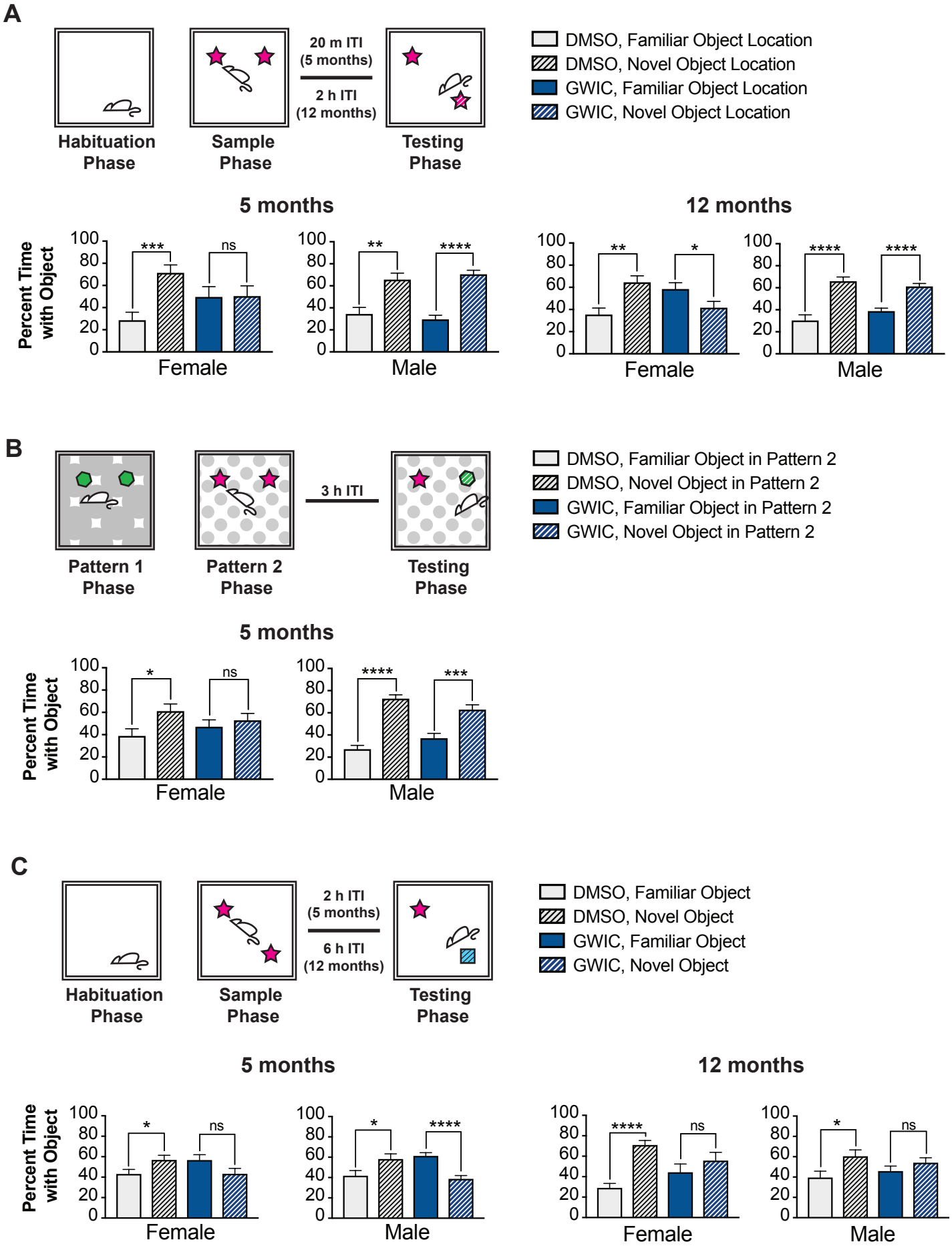

649 **Figure 1. Exposure of C57BL/6 wild-type mice to GWIC results in sex-dependent**
650 **impairments in spatial memory, pattern separation, and novel object recognition.** (A) The
651 diagram in the top panel depicts the sequential phases used in the object location test (OLT): the
652 habituation phase, the sample phase, and the testing phase. Each phase lasted five minutes, and the
653 inter-trial interval (ITI) between the sample and testing phase was 20 minutes (5 months post-
654 exposure) or 2 hours (12 months post-exposure). The bar graphs in the bottom panel compare the
655 percentages of total exploration time spent with the object in the familiar location versus time spent
656 with the object in the novel location for both the OLT conducted 5 months and 12 months post-
657 exposure, for DMSO- and GWIC-exposed female and male mice. (B) The diagram in the top panel
658 depicts the sequential phases used in the pattern separation test (PST): the Pattern 1 phase, the
659 Pattern 2 phase, and the testing phase, in which one of the objects from Pattern 1 was placed into
660 Pattern 2. Each phase lasted five minutes, and the inter-trial interval (ITI) between the sample and
661 testing phase was 3 hours. The bar graphs in the bottom panel compare the percentages of total
662 exploration time spent with the familiar object in Pattern 2 versus time spent with the novel object
663 in Pattern 2 for a PST conducted 5 months post-exposure, for DMSO- and GWIC-exposed female
664 and male mice. (C) The diagram in the top panel depicts the sequential phases used in the novel
665 object recognition test (NORT): the habituation phase, the sample phase, and the testing phase.
666 Each phase lasted five minutes, and the inter-trial interval (ITI) between the sample and testing
667 phase was 2 hours (5 months post-exposure) or 6 hours (12 months post-exposure). The bar graphs
668 in the bottom panel compare the percentages of total exploration time spent with the familiar object
669 versus time spent with the novel object both the NORT conducted 5 months and 12 months post-
670 exposure, for DMSO- and GWIC-exposed female and male mice.). Error bars represent the mean

671 of biological replicates +/- SEM (n=9-10). Indicated p-values were calculated two-tailed, unpaired,

672 Student's t-test. *$p < 0.05$; **$p < 0.01$; ***$p < 0.001$; ****$p < 0.0001$; ns, not significant.

Figure 2. Exposure of C57BL/6 wild-type mice to GWIC results in sex-dependent alterations in expression of mitochondrial proteins in the hippocampus and cerebral cortex.

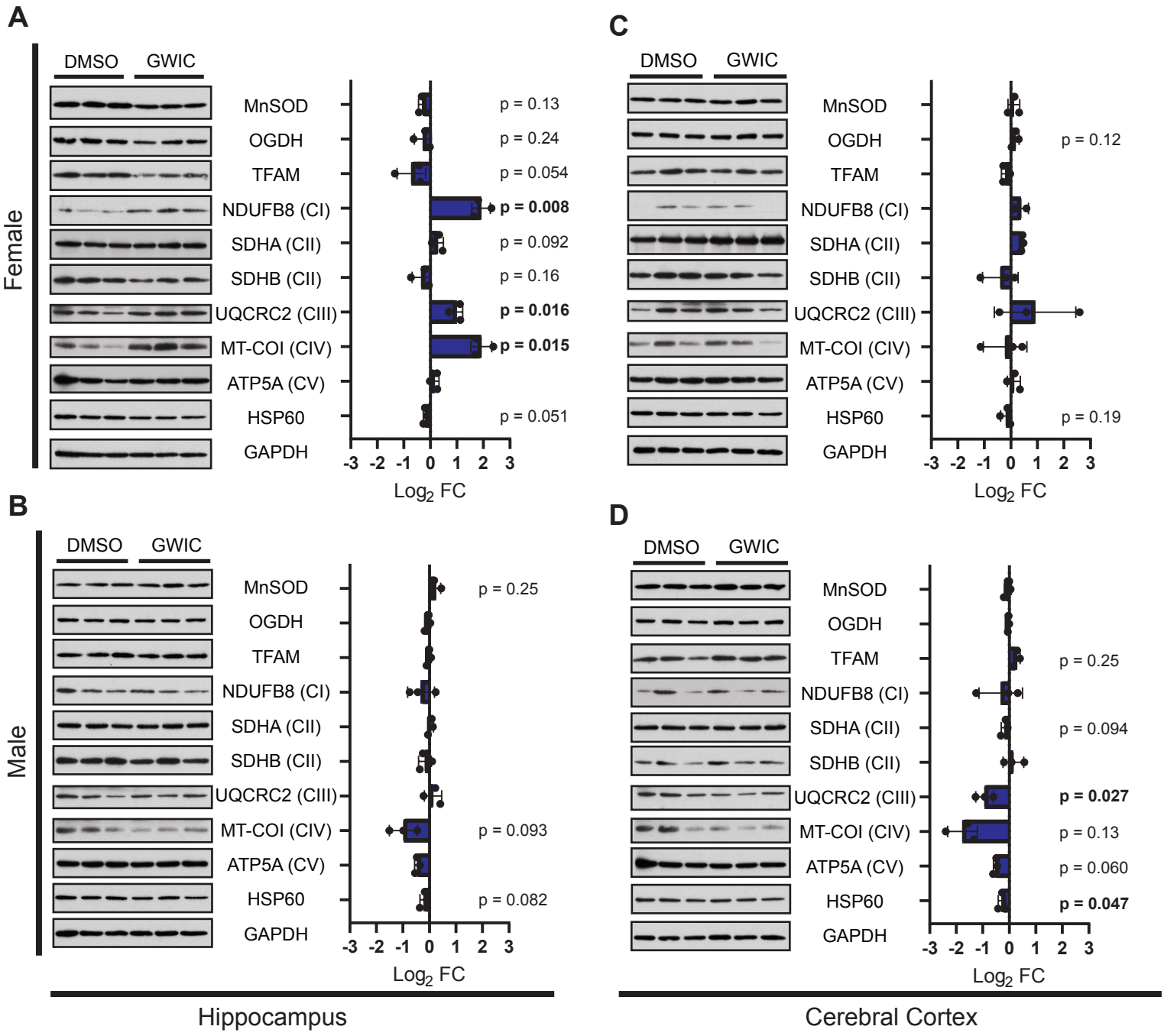

673 **Figure 2. Exposure of C57BL/6 wild-type mice to GWIC results in sex-dependent alterations**
674 **in expression of mitochondrial proteins in the hippocampus and cerebral cortex.** At 12
675 months post-exposure, tissue extracts were generated from microdissected hippocampi from
676 DMSO- and GWIC-exposed female mice (A) and male mice (B) and from cerebral cortex samples
677 from DMSO- or GWIC-exposed female mice (C) and male mice (D), and immunoblotted for the
678 listed proteins as described in Section 2.5 of materials and methods. Labels in parentheses next to
679 listed proteins designate proteins as part of complex I (CI), complex II (CII), complex III (CIII),
680 complex IV (CIV) or complex V (CV) of the electron transport chain. Densitometry for each
681 protein was performed in ImageJ and normalized to the GAPDH expression level. Bars represent
682 the $\log_2$ fold change (FC) of biological replicates +/- SD (n=3). Indicated p-values were calculated
683 using a two-tailed t test, and values below 0.05 are shown in bold.

Figure 3. Increased astrocyte hypertrophy is observed in three hippocampal regions of female GWIC-exposed mice and in two hippocampal regions of male GWIC-exposed mice.

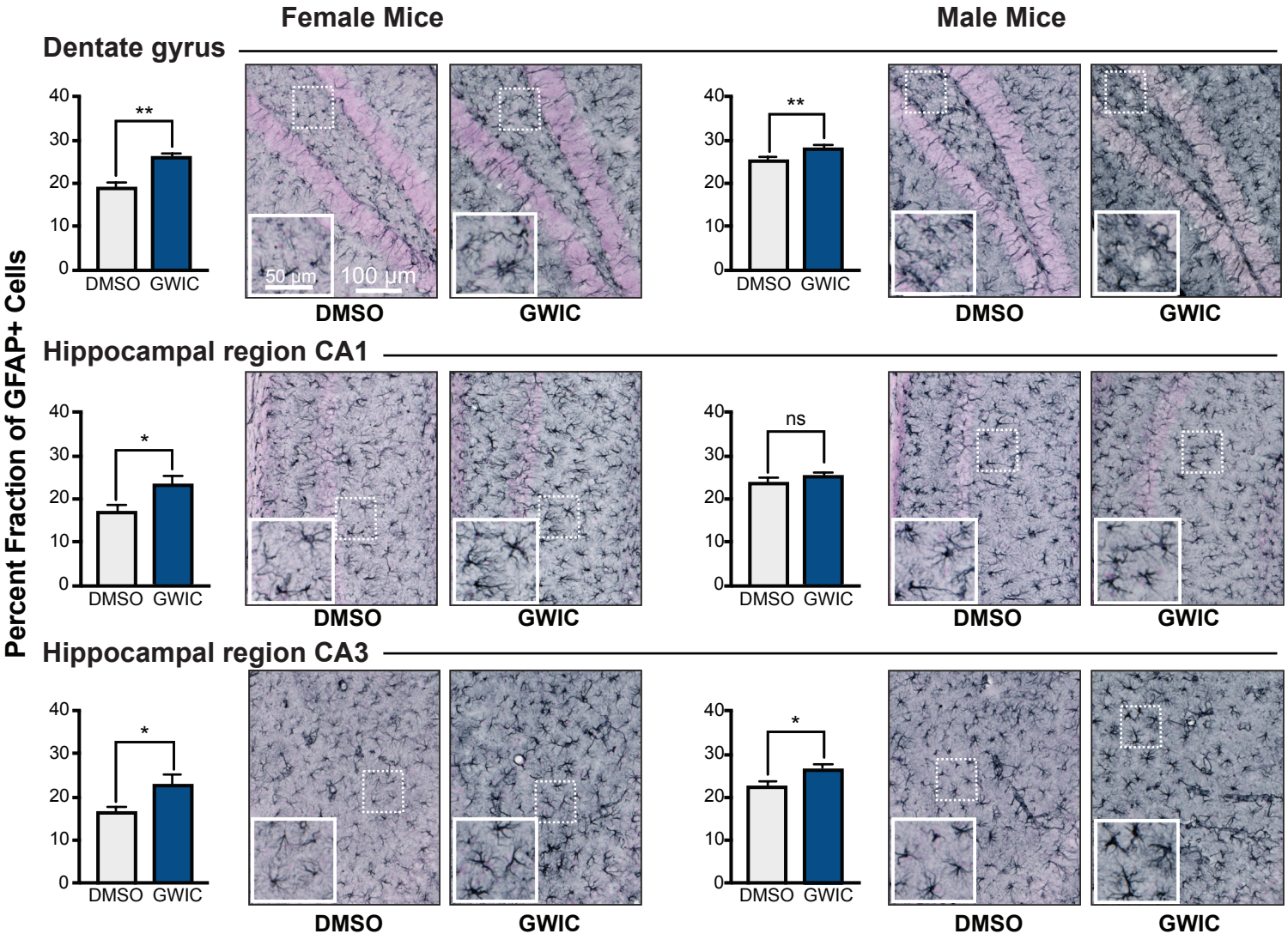

684 **Figure 3. Increased astrocyte hypertrophy is observed in three hippocampal regions of**
685 **female GWIC-exposed mice and in two hippocampal regions of male GWIC-exposed mice.**
686 We measured percent fraction of glial-fibrillary acidic protein-expressing (GFAP+) cells within
687 three regions of the hippocampus: the dentate gyrus (DG), CA1, and CA3. Images show
688 representative distribution and morphology of GFAP+ astrocytes in these three regions in male
689 and female GWIC-exposed and DMSO-exposed mice (scale bar = 100 μM). Insets show magnified
690 views (scale bar = 50 μM); adjacent bar graphs show quantification of percent fraction GFAP+ for
691 each cohort). Error bars represent the mean of biological replicates +/- SEM (n=6). Indicated p-
692 values were calculated using two-tailed, unpaired, Student's t-test.. *$p < 0.05$; **$p < 0.01$; ns, not
693 significant.

Figure 4. GWIC-exposure alters mitochondrial respiration and potentiates inflammatory responses in BMDMs.

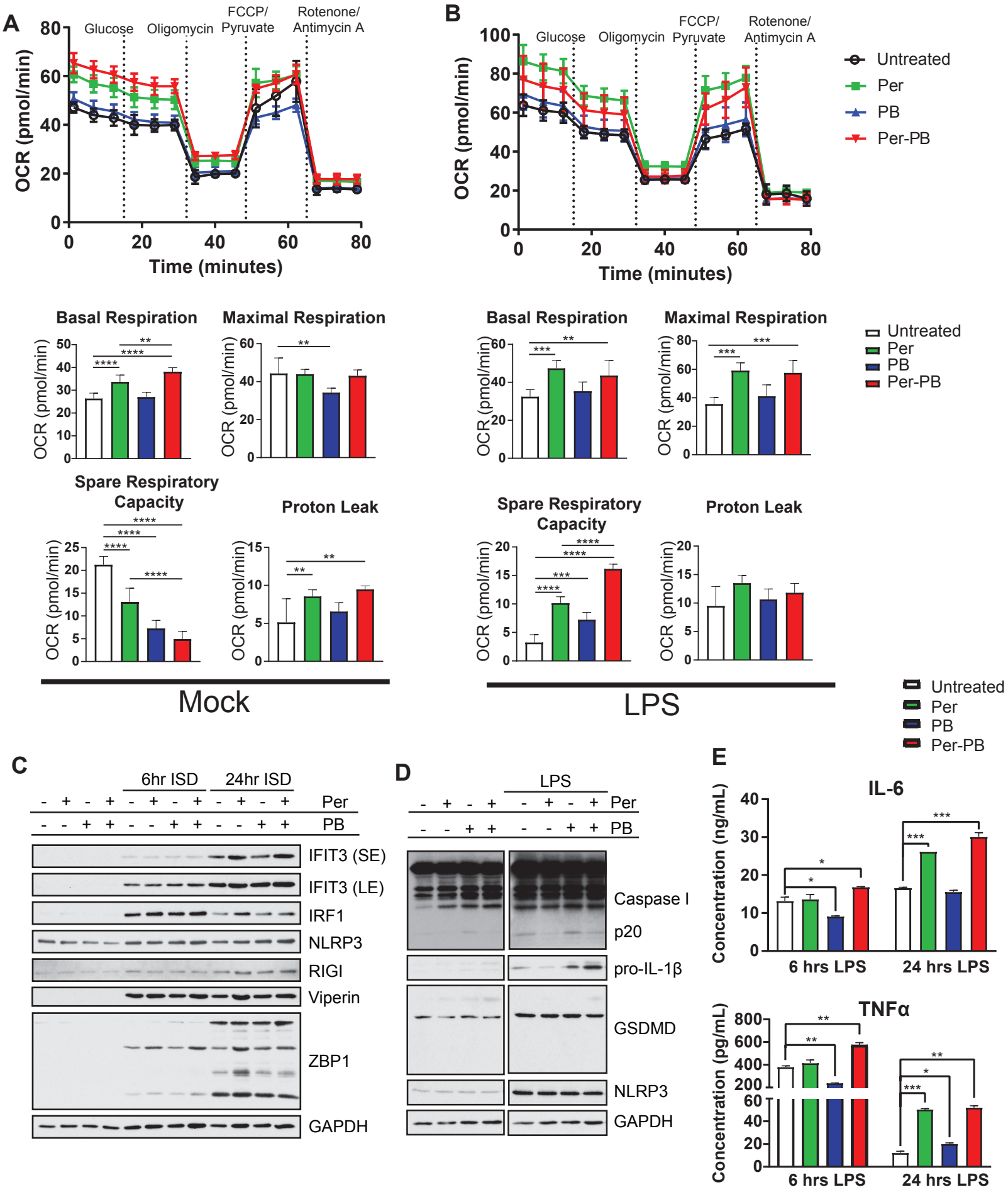

694 **Figure 4. GWIC exposure alters mitochondrial respiration and potentiate inflammatory**
695 **responses in BMDMs.** (A) and (B) Oxygen consumption rate (OCR) in BMDMs treated with
696 GWIC. BMDMs were treated overnight with GWIC as indicated. Cells were treated with (A)
697 Seahorse medium (Mock) or (B) 200 ng/mL LPS (LPS) for 6 hours, then respiration was measured
698 on a Seahorse XF96 Analyzer using a modified protocol as described in Section 2.8 of materials
699 and methods. (C) ISG expression in BMDMs treated with GWIC and transfected with ISD.
700 BMDMs were treated overnight with GWIC as indicated, then transfected with 1 μg ISD for 6 or
701 24 hours. Cells extracts were blotted for indicated proteins as in Figure 2. (D) Inflammasome
702 activation in BMDMs treated with GWIC. BMDMs were treated overnight with GWIC as
703 indicated, then treated with 20 ng/mL LPS for 6 or 24 hours. Cells extracts were blotted for
704 indicated proteins as in Figure 2. (E) ELISA of inflammatory cytokines in BMDMs treated as in
705 (D). Data shown is representative of three separate experiments. Error bars represent the mean of
706 technical replicates +/- SD (n=5 for (A) and (B) and n=2 for (E)). Significance values for pairwise
707 comparisons were calculated using the two-stage step-up method to yield q values that have been
708 corrected for the false discovery rate. * $q < 0.05$; ** $q < 0.01$; *** $q < 0.001$; **** $q < 0.0001$.

Figure 5. Loss of STING attenuates GWIC-related neurobehavioral changes, neuroinflammation, and mitochondrial rewiring.

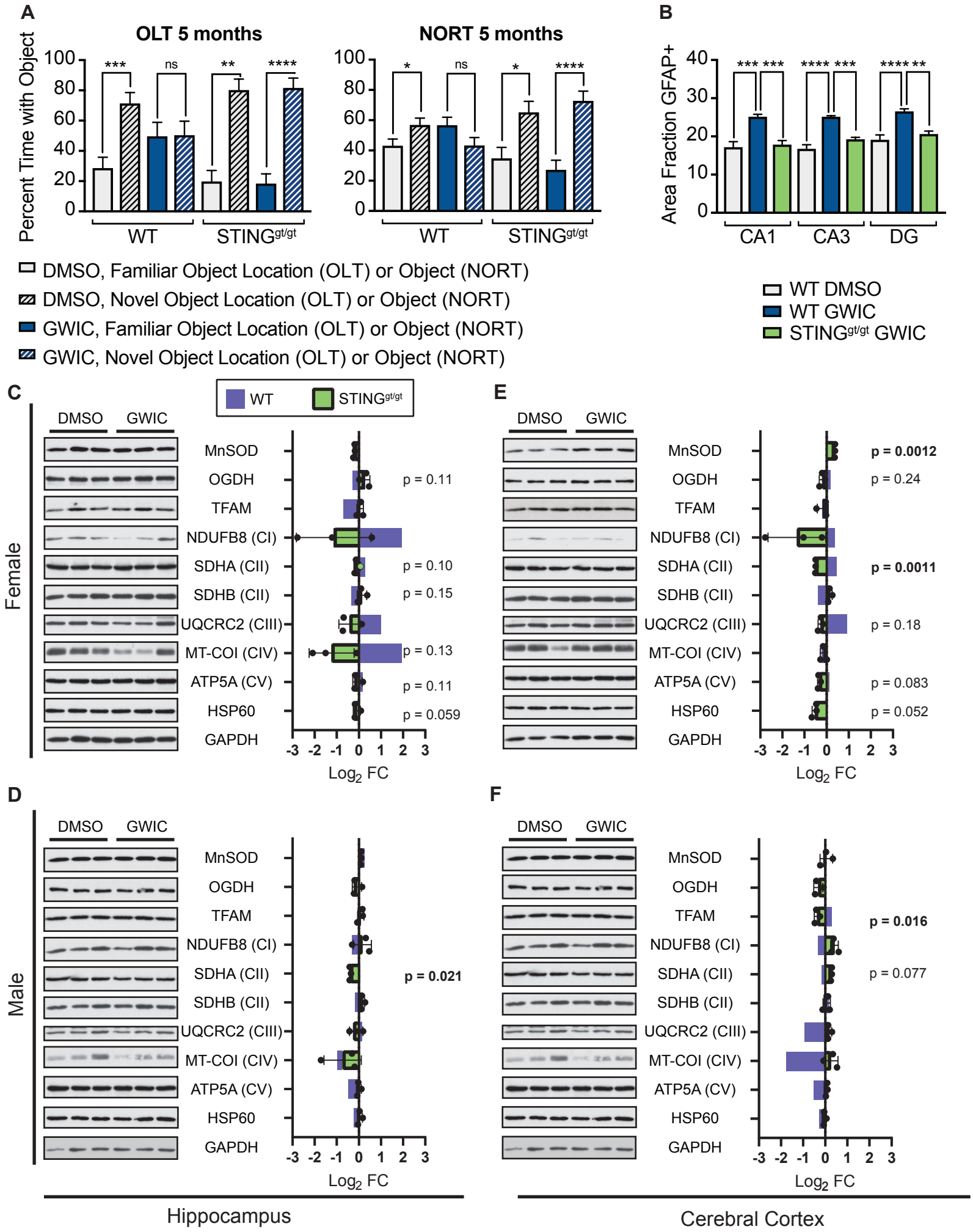

709 **Figure 5. Loss of STING attenuates GWIC-related neurobehavioral changes,**
710 **neuroinflammation, and mitochondrial rewiring.** (A) A comparison of OLT and NORT results
711 in DMSO- or GWIC-exposed WT and STING$^{gt/gt}$ C57BL/6 female mice. Error bars represent the
712 mean of biological replicates +/- SEM (OLT: n=3 for DMSO control mice, n=6 for GWIC-exposed
713 mice; NORT; n=4 for DMSO control mice, n=8 for GWIC-exposed mice). (B) Comparison of
714 percent fraction of GFAP+ cells within the dentate gyrus (DG), CA1, and CA3 of DMSO- or
715 GWIC-exposed WT female mice and GWIC-exposed STING$^{gt/gt}$ female mice. Indicated p-values
716 for (A) and (B) were calculated using two-tailed, unpaired, Student's t-test. *$p < 0.05$; **$p < 0.01$;
717 ***$p < 0.001$; ****$p < 0.0001$; ns, not significant. (C) Hippocampal extracts from DMSO- and
718 GWIC-exposed female (C) and male (D) WT and STING$^{gt/gt}$ mice and cerebral cortex extracts
719 from DMSO- and GWIC-exposed female (E) and male (F) WT and STING$^{gt/gt}$ mice 12 months
720 post-exposure were generated and blotted as described in Figure 2. Green bars represent the $\log_2$
721 fold change (FC) of biological replicates +/- SD (n=3) of STING$^{gt/gt}$ extracts, with each replicate
722 represented by a black dot. Blue bars in overlay represent the $\log_2$ fold change (FC) of biological
723 replicates (n=3) of WT samples from Figure 2, for sake of comparison. Densitometry for each
724 protein was performed in ImageJ and normalized to the GAPDH expression level. Indicated p-
725 values, which refer to STING$^{gt/gt}$ samples, were calculated using a two-tailed t test, and values
726 below 0.05 are shown in bold.

Figure 6. Loss of NLRP3 attenuates GWIC-related neurobehavioral changes, neuroinflammation, and mitochondrial rewiring.

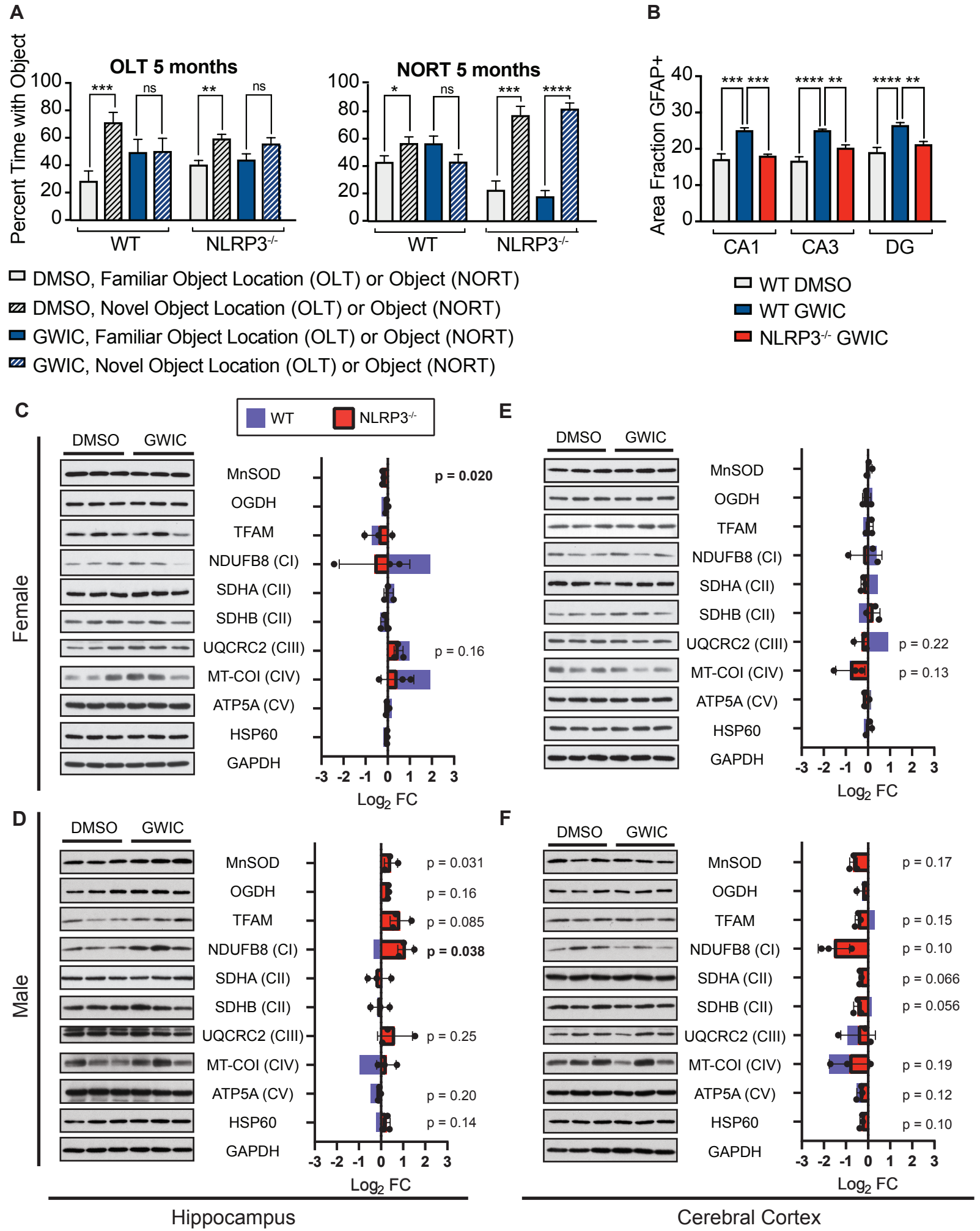

727 **Figure 6. Loss of NLRP3 (partly) attenuates GWIC-related neurobehavioral changes,**
728 **neuroinflammation, and mitochondrial rewiring. (A)** A comparison of OLT and NORT results
729 in DMSO- or GWIC-exposed WT and NLRP3$^{-/-}$ C57BL/6 female mice. Error bars represent the
730 mean of biological replicates +/- SEM (OLT: n=5 for DMSO control mice, n=10 for GWIC-
731 exposed mice; NORT; n=5 for DMSO control mice, n=9 for GWIC-exposed mice). (B)
732 Comparison of percent fraction of GFAP+ cells within the dentate gyrus (DG), CA1, and CA3 of
733 DMSO- or GWIC-exposed WT female mice and GWIC-exposed NLRP3$^{-/-}$ female mice. Indicated
734 p-values for (A) and (B) were calculated using two-tailed, unpaired, Student's t-test. *$p < 0.05$;
735 **$p < 0.01$; ***$p < 0.001$; ****$p < 0.0001$. (C) Hippocampal extracts from DMSO- and GWIC-
736 exposed female (C) and male (D) WT and NLRP3$^{-/-}$ mice and cerebral cortex extracts from DMSO-
737 and GWIC-exposed female (E) and male (F) WT and NLRP3$^{-/-}$ mice 12 months post-exposure
738 were generated and blotted as described in Figure 2. Red bars represent the $\log_2$ fold change (FC)
739 of biological replicates +/- SD (n=3) of NLRP3$^{-/-}$ extracts, with each replicate represented by black
740 dots. Blue bars in overlay represent the $\log_2$ fold change (FC) of biological replicates (n=3) of WT
741 samples from Figure 2, for sake of comparison. Densitometry for each protein was performed in
742 ImageJ and normalized to the GAPDH expression level. Indicated p-values, which refer to NLRP3^{-}
743 $^{/-}$ samples, were calculated using a two-tailed t test, and values below 0.05 are shown in bold.

Supplemental Figure 1. Control data for OLT (object location test), PST (pattern separation test), and NORT (novel object recognition test) experiments depicted in Figure 1: total object exploration time, distance moved, and velocity.

Object Location Test
5 months

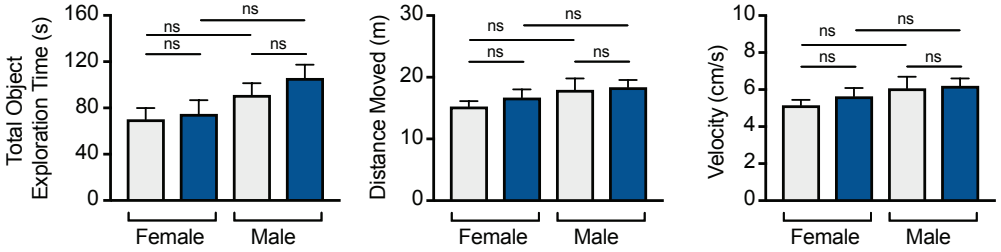

Object Location Test
12 months

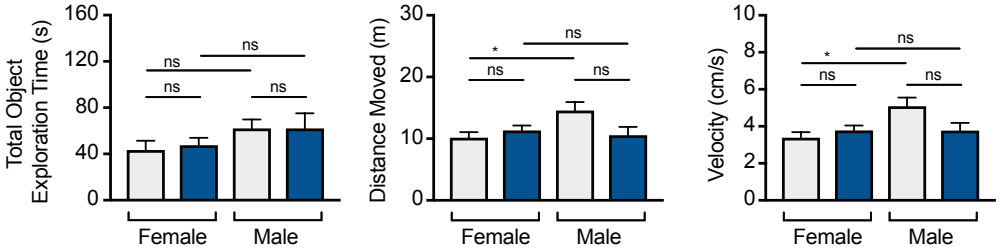

Pattern Separation Test
5 months

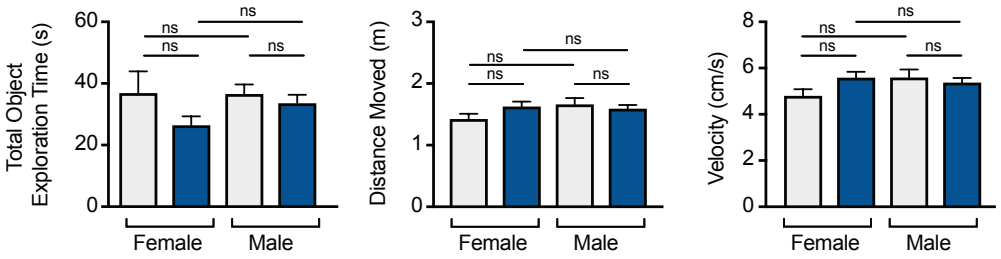

Novel Object Recognition Test
5 months

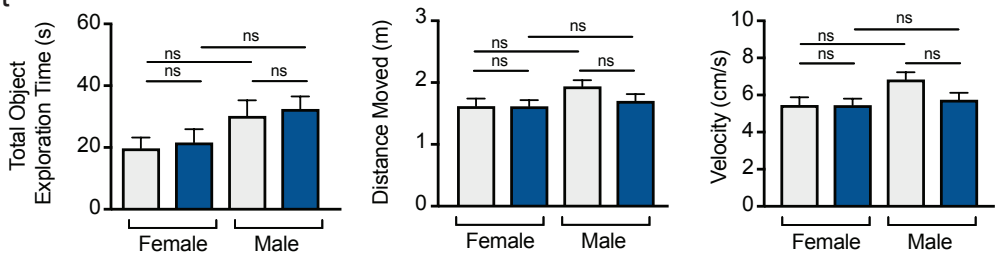

Novel Object Recognition Test
12 months

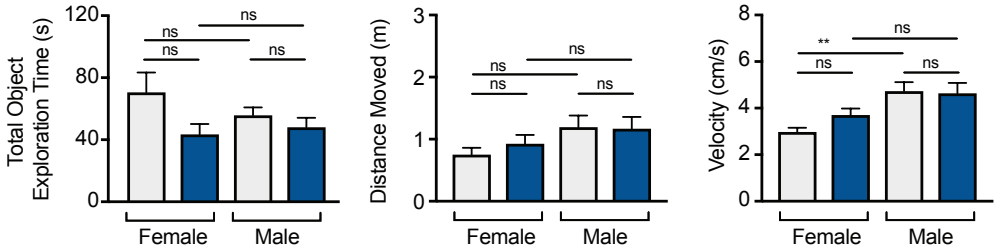

744 **Supplemental Figure 1. Control data for OLT (object location test), PST (pattern separation**
745 **test), and NORT (novel object recognition test) experiments depicted in Figure 1: total object**
746 **exploration time, distance moved, and velocity.** For all the neurobehavioral tests (OLT, PST,
747 and NORT) depicted in Figure 1, data were collected on total object exploration time (seconds),
748 distance moved (meters), and velocity (centimeters per second) of all mice for all three tests (object
749 location test, OLT; pattern separation test, PST; novel object recognition test, NORT). Error bars
750 represent the mean of biological replicates +/- SEM (n=9-10). Indicated p-values were calculated
751 using one-way ANOVA with Tukey's multiple comparison. *$p < 0.05$; **$p < 0.01$; ns, not
752 significant.

Supplemental Figure 2. The elevated plus maze test (EPMT) was used at 5 months post exposure to assess anxiety-related behavior in all cohorts.

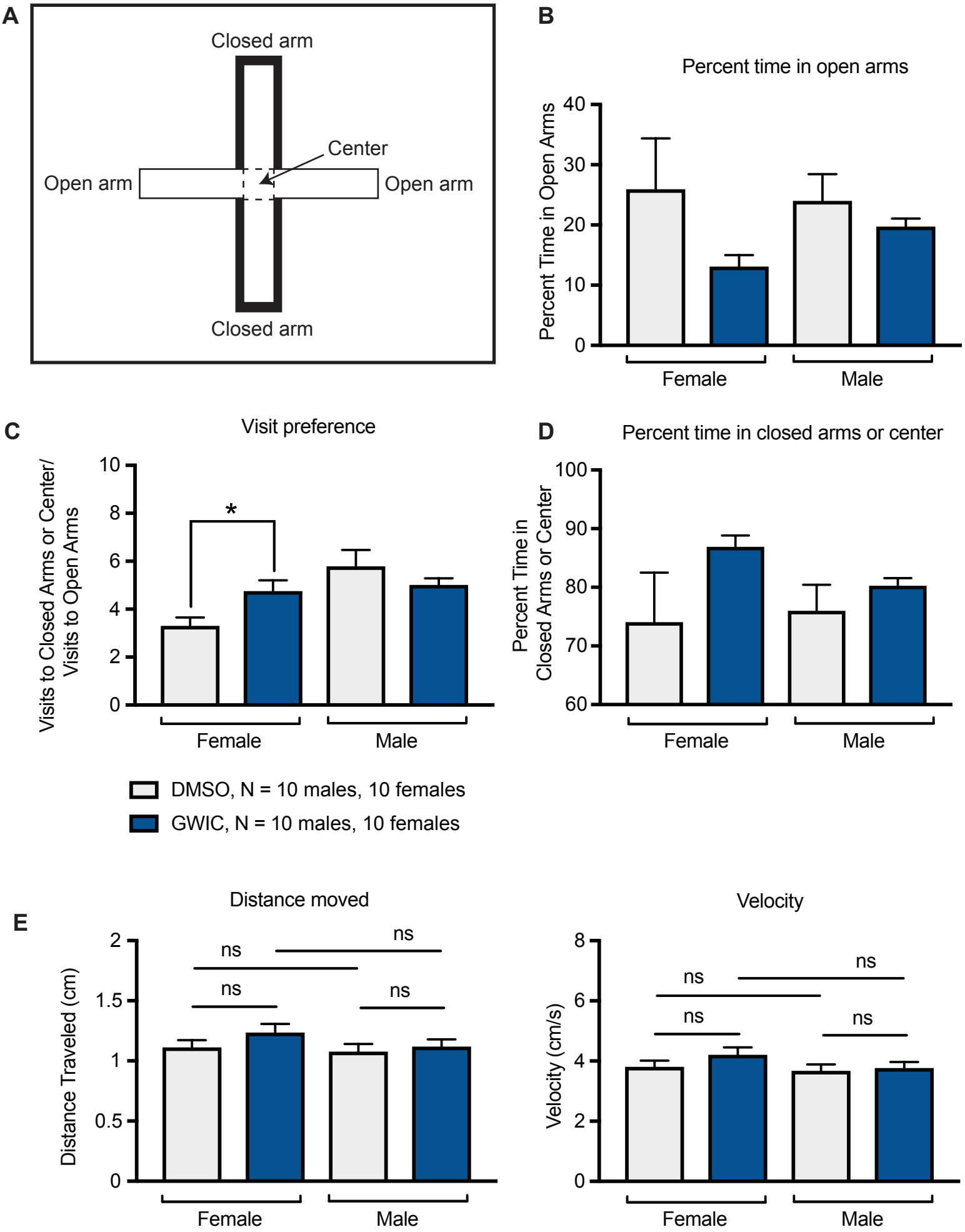

753 **Supplemental Figure 2. The elevated plus maze test (EPMT) was used at 5 months post-**
754 **exposure to assess anxiety-related behavior in all cohorts**. (A) The diagram depicts the
755 experimental setup for this test: a 60 cm elevated plus-shaped apparatus with four arms, each 35
756 cm in length and 5 cm in width. Two of the arms are surrounded with walls on three sides of 15
757 cm in height (the two regions identified as "closed arm" in the diagram) and two of the arms are
758 open (the two regions identified as "open arm" in the diagram). Mice are gently placed in the
759 region identified as "center" in the diagram, facing a closed arm, and allowed to freely explore the
760 maze for one five minute interval. (B) Percent time spent in the open arms was calculated and
761 compared among cohorts. (C) Visits to each region were also calculated, as was visit preference,
762 calculated as the ratio of number of visits to the closed arms or the center and the number of visits
763 to the open arms. (D) Percent time spent in the closed arms or center was calculated and compared
764 among cohorts. (E) Distance moved and velocity of all mice during the test. Error bars represent
765 the mean of biological replicates +/- SEM (n=10). Indicated p-values were calculated using two-
766 tailed, unpaired, Student's t-test. *$p < 0.05$; ns, not significant.

Supplementary Figure 3. ISG expression, inflammasome activation, and glycolysis in BMDMs treated with GWICs.

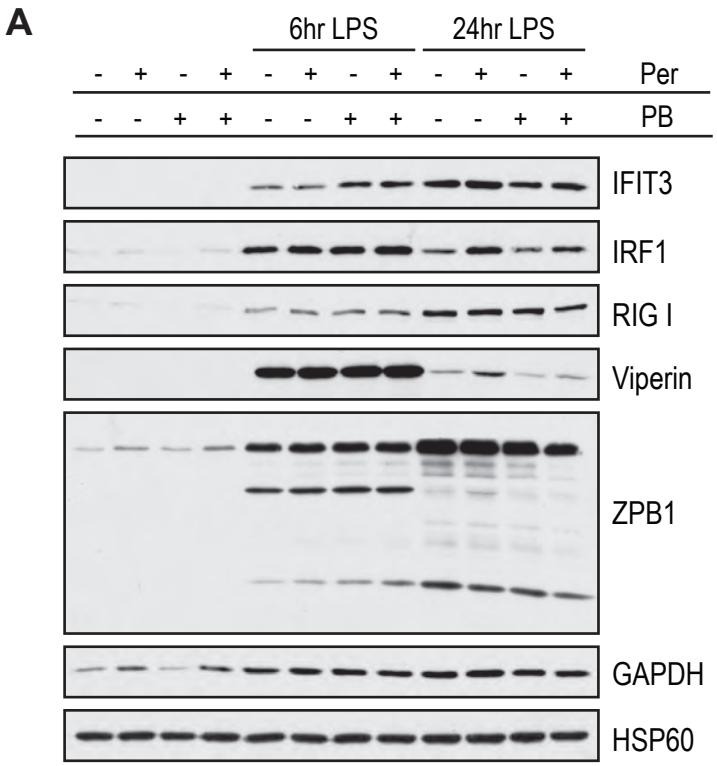

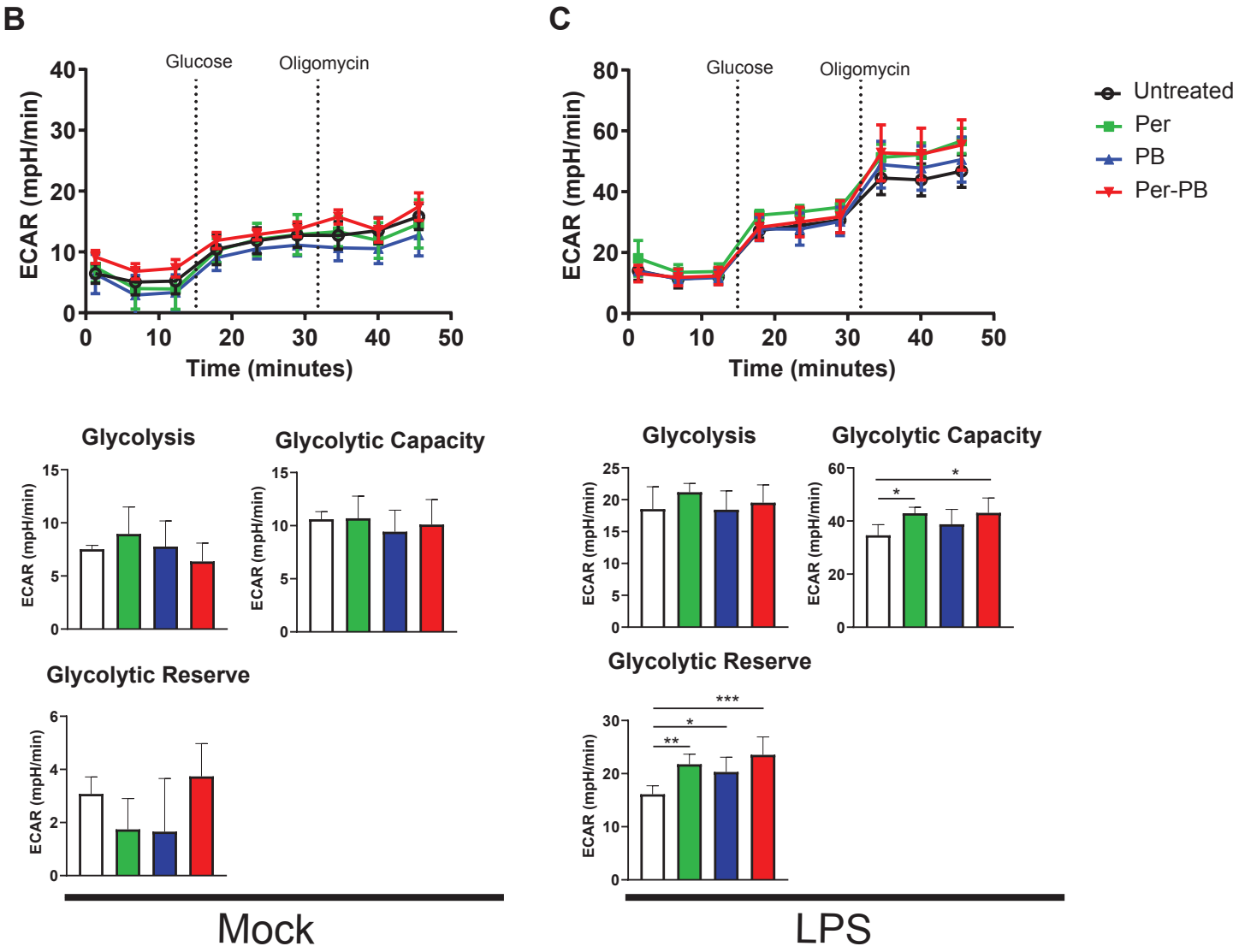

767 **Supplemental Figure 3. ISG expression, inflammasome activation, and glycolysis in BMDMs**
768 **treated with GWIC.** (A) Western blot analysis of ISG expression in BMDMs treated with
769 overnight with GWIC, then treated with 200 ng/mL LPS for 6 or 24 hours as indicated. Cells
770 extracts were blotted for indicated proteins as in Figure 2. (B) and (C) Glycolysis as measured by
771 extracellular acidification rate (ECAR) in BMDMs treated with GWIC. BMDMs were treated
772 overnight with GWIC as indicated. Cells were treated with Seahorse medium (Mock) (B) or 200
773 ng/mL LPS (LPS) for 6 hours (C), then ECAR was measured on a Seahorse XF96 Analyzer using
774 a modified protocol as described in Section 2.8 of materials and methods. Error bars represent the
775 mean of technical replicates +/- SD (n=5). Significance values for pairwise comparisons were
776 calculated using the two-stage step-up method to yield q values that have been corrected for the
777 false discovery rate. * $q < 0.05$; ** $q < 0.01$; *** $q < 0.001$; **** $q < 0.0001$.

Supplemental Figure 4. Addition neurobehavioral tests performed on DMSO- and GWIC-exposed NLRP3$^{-/-}$STING$^{gt/gt}$ C57BL/6 female mice.

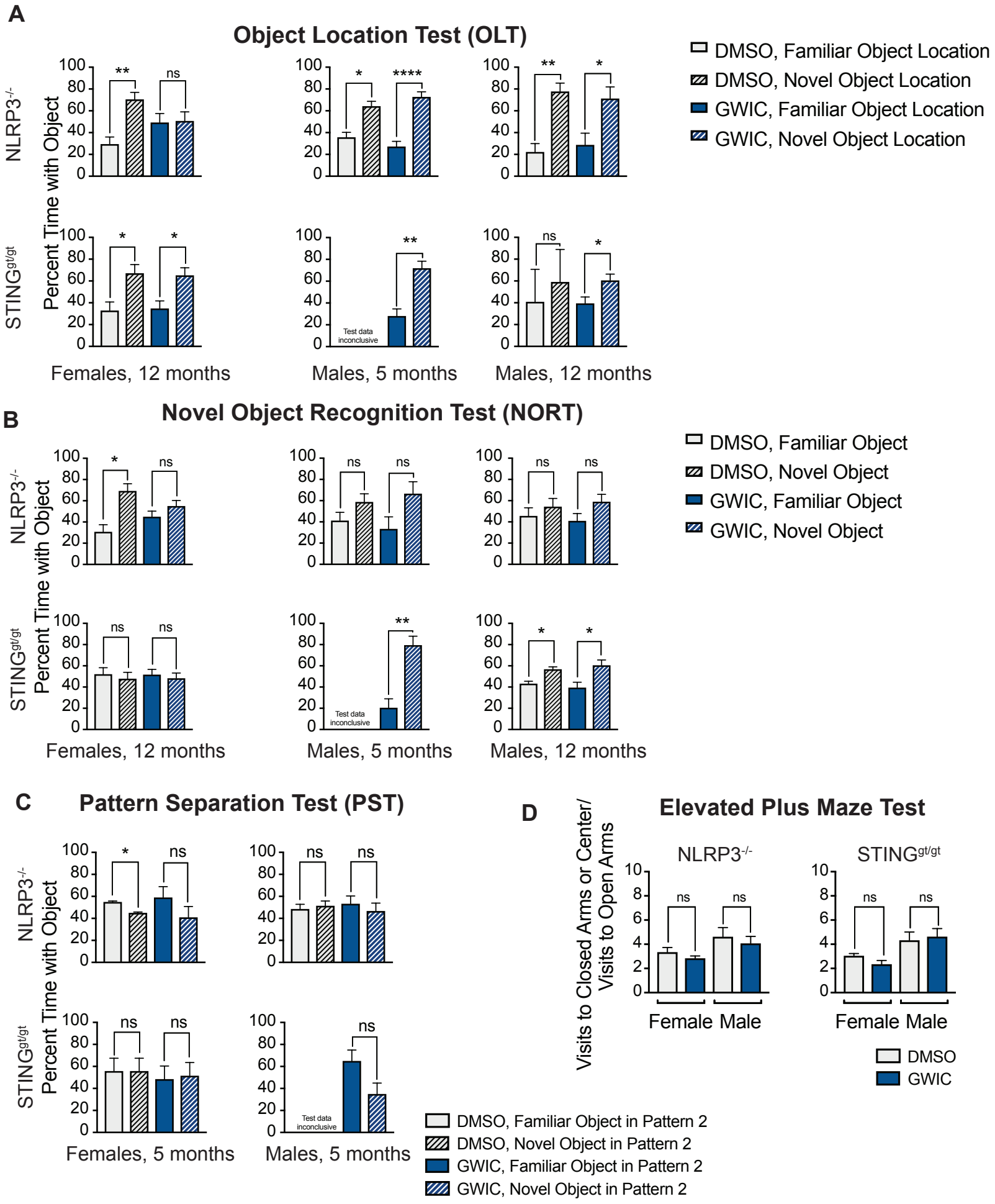

778 **Supplemental Figure 4. Additional neurobehavioral tests performed on DMSO- and GWIC-**
779 **exposed NLRP3$^{-/-}$ and STING$^{gt/gt}$ C57BL/6 female mice.** (A) Results of OLT testing on DMSO-
780 and GWIC-exposed female NLRP3$^{-/-}$and STING$^{gt/gt}$ mice at 12 months post-exposure and DMSO-
781 and GWIC-exposed male NLRP3$^{-/-}$and STING$^{gt/gt}$ mice at 5 and 12 months post-exposure.
782 Experiments were performed as in Figure 1. (B) Results of NORT testing on DMSO- and GWIC-
783 exposed female NLRP3$^{-/-}$and STING$^{gt/gt}$ mice at 12 months post-exposure and DMSO- and GWIC-
784 exposed male NLRP3$^{-/-}$and STING$^{gt/gt}$ mice at 5 and 12 months post-exposure. Experiments were
785 performed as in Figure 1. (C) Results of PST testing on DMSO- and GWIC-exposed female and
786 male NLRP3$^{-/-}$and STING$^{gt/gt}$ mice at 5 and 12 months post-exposure. Experiments were
787 performed as in Figure 1. (D) Results of EPMT testing on DMSO- and GWIC-exposed female and
788 male NLRP3$^{-/-}$and STING$^{gt/gt}$ mice at 5 months post-exposure. Experiments were performed as in
789 Supplemental Figure 2. Error bars represent the mean of biological replicates +/- SEM (n=5-10 for
790 STING$^{gt/gt}$ females and 3-6 for STING$^{gt/gt}$ males, n=5-10 for NLRP3$^{-/-}$females and 3-7 for NLRP3^{-}
791 $^{/-}$males). Indicated p-values were calculated using two-tailed, unpaired, Student's t-test. * $p < 0.05$;
792 ** $p < 0.01$; **** $p < 0.0001$, ns, not significant.

Supplemental Figure 5. Control data for OLT (object location test), PST (pattern separation test), and NORT (novel object recognition test) experiments depicted in Figures 5 and 6: total object exploration time, distance moved, and velocity for STING$^{gt/gt}$ and NLRP3$^{-/-}$ mice.

STING$^{gt/gt}$

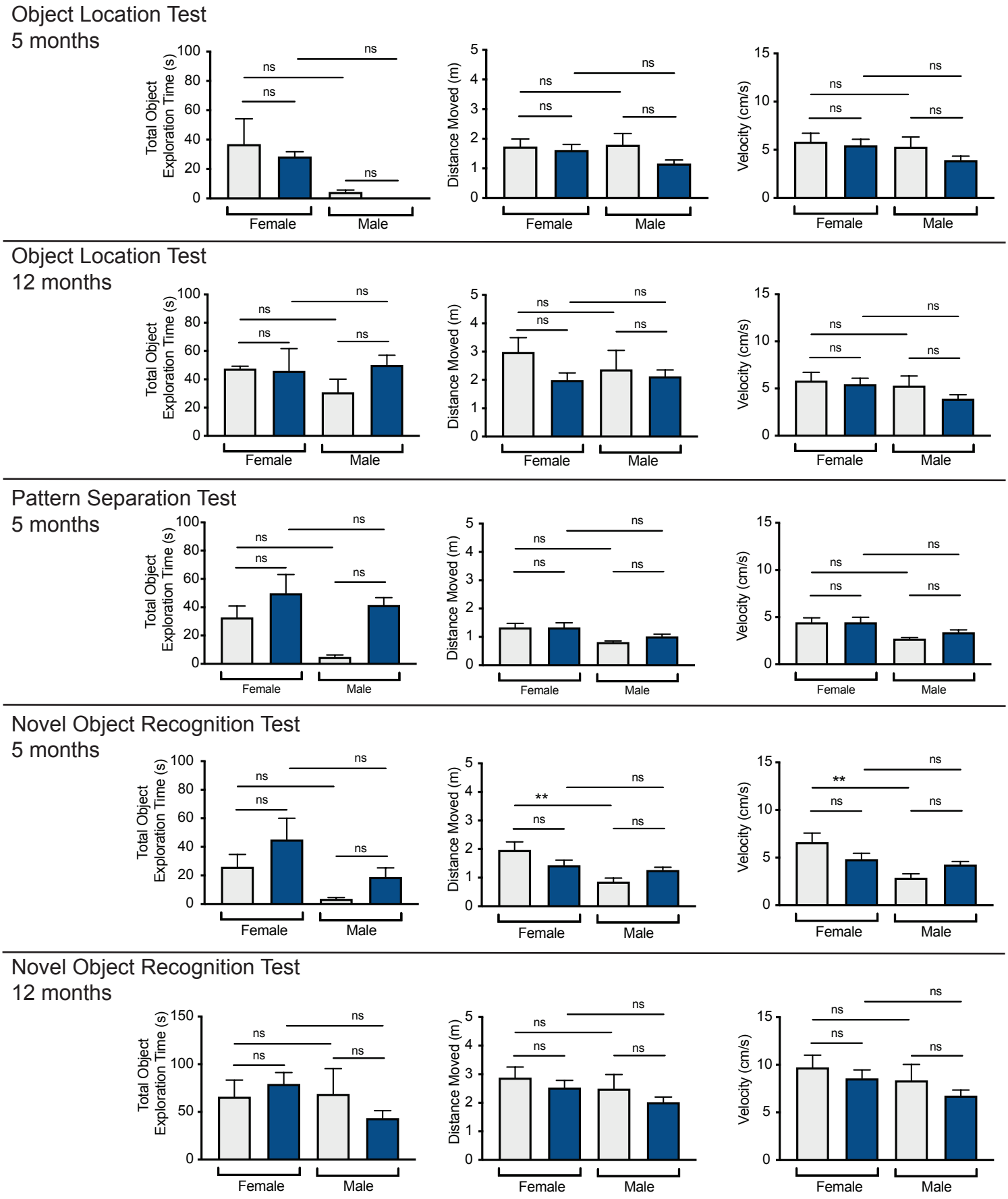

Supplemental Figure 5. Control data for OLT (object location test), PST (pattern separation test), and NORT (novel object recognition test) experiments depicted in Figures 5 and 6: total object exploration time, distance moved, and velocity for STING$^{gt/gt}$ and NLRP3$^{-/-}$ mice.

NLRP3$^{-/-}$

Object Location Test
5 months

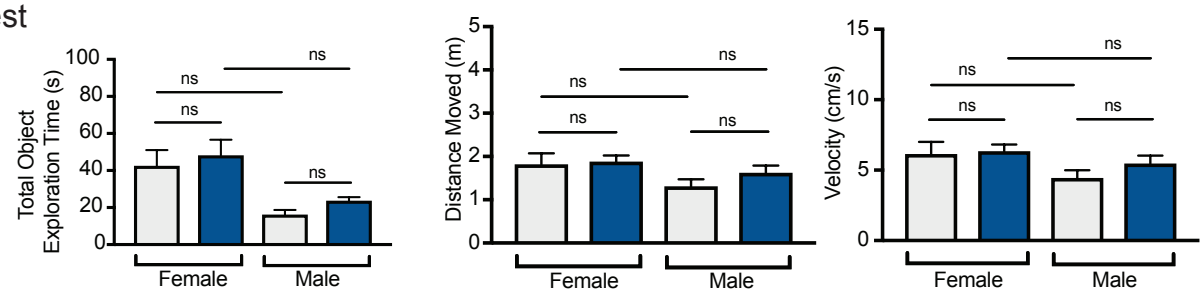

Object Location Test
12 months

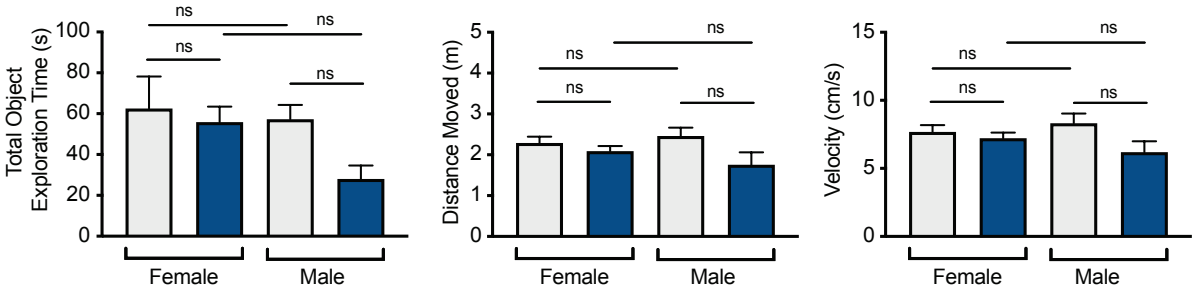

Pattern Separation Test
5 months

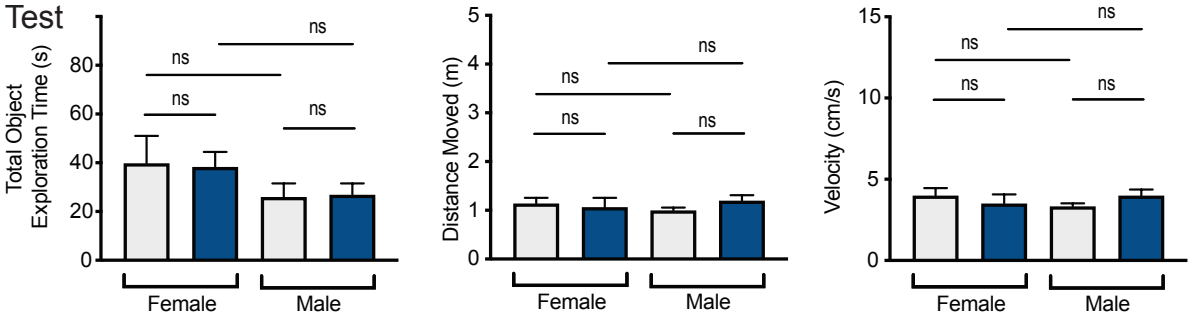

Novel Object Recognition Test
5 months

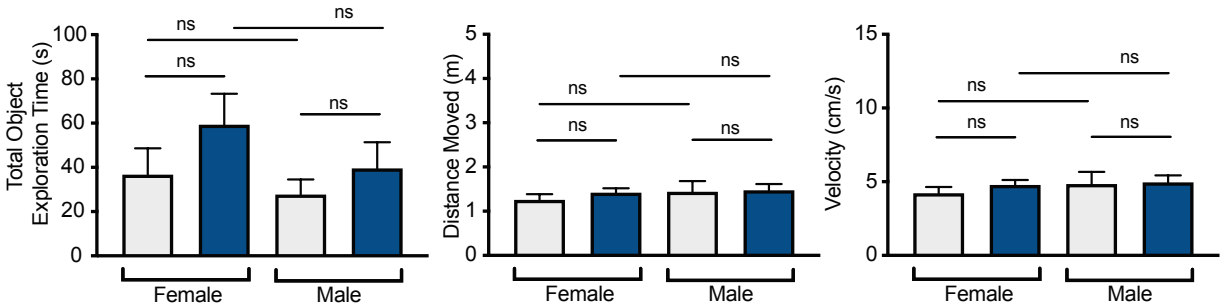

Novel Object Recognition Test
12 months

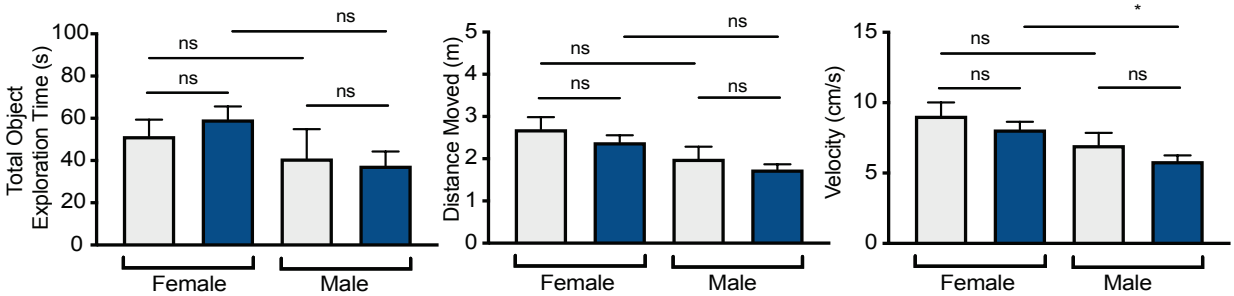

Supplemental Figure 5. Control data for OLT (object location test), PST (pattern separation test), and NORT (novel object recognition test): total object exploration time, distance moved, and velocity for STING$^{gt/gt}$ and NLRP3$^{-/-}$ mice. For the OLT, PST, and NORT data depicted in Figures 5, 6, and Supplemental Figure 4, data were collected on total object exploration time (seconds), distance moved (meters), and velocity (centimeters per second) of all mice for all three tests (object location test, OLT; pattern separation test, PST; novel object recognition test, NORT). Error bars represent the mean of biological replicates +/- SEM (n=5-10 for STING$^{gt/gt}$ females and 3-6 for STING$^{gt/gt}$ males, n=5-10 for NLRP3$^{-/-}$females and 3-7 for NLRP3$^{-/-}$males). Indicated p-values were calculated using one-way ANOVA with Tukey's multiple comparisons. *$p < 0.05$; **$p < 0.01$; ns, not significant.

Supplementary Figure 6. Percent fraction of GFAP+ cells and GFAP expression in the hippocampi of NLRP3$^{-/-}$ and STING$^{gt/gt}$ GWIC-exposed female mice

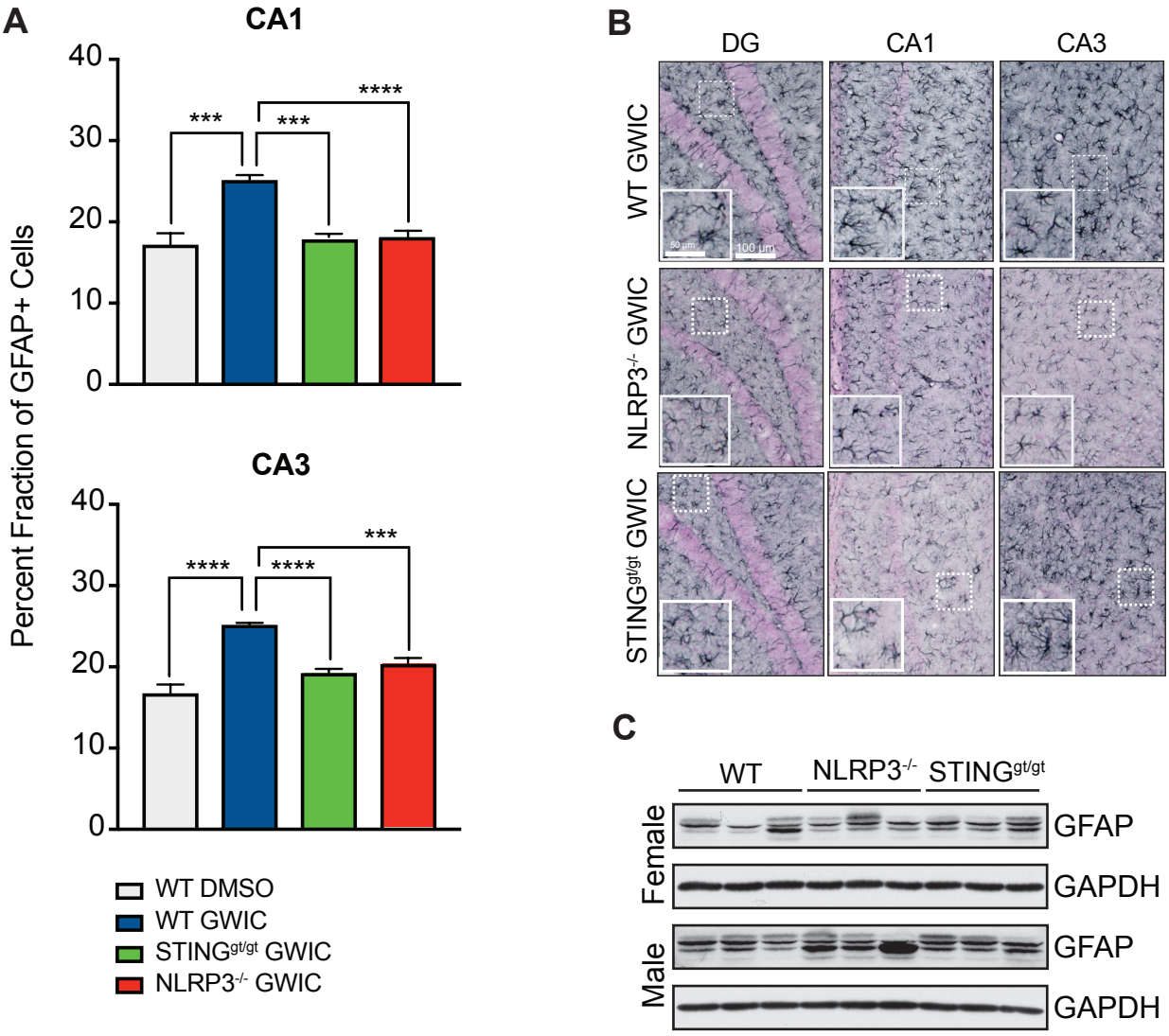

803 **Supplementary Figure 6. Percent fraction of GFAP+ cells and GFAP expression in the**
804 **hippocampi of NLRP3$^{-/-}$ and STING$^{gt/gt}$ female mice. (A)** Quantification of percent fraction
805 GFAP+ cells within two regions of the hippocampus (the CA1 and CA3) in DMSO-exposed WT
806 female mice and GWIC-exposed WT, NLRP3$^{-/-}$ and STING$^{gt/gt}$ female mice. Error bars represent
807 the mean of biological replicates +/- SEM (n=6). Indicated p-values were calculated using two-
808 tailed, unpaired, Student's t-test. ***$p < 0.001$; **** $p < 0.0001$. (B) Images show representative
809 distribution and morphology of GFAP+ astrocytes in these three regions in female GWIC-exposed
810 WT, NLRP3$^{-/-}$ and STING$^{gt/gt}$ mice (scale bar = 100 μM). Insets show magnified views (scale bar
811 = 50 μM). (C) Tissue extracts were generated from microdissected hippocampi from DMSO-
812 exposed WT, NLRP3$^{-/-}$ and STING$^{gt/gt}$ mice and immunoblotted for GFAP as described in
813 Materials and Methods. Each lane represents one mouse, with n=3 for each genotype and sex.

Supplementary Figure 7. Analysis and imaging of IBA-1+ cells in the hippocampi of WT, NLRP3$^{-/-}$ and STING$^{gt/gt}$ mice.

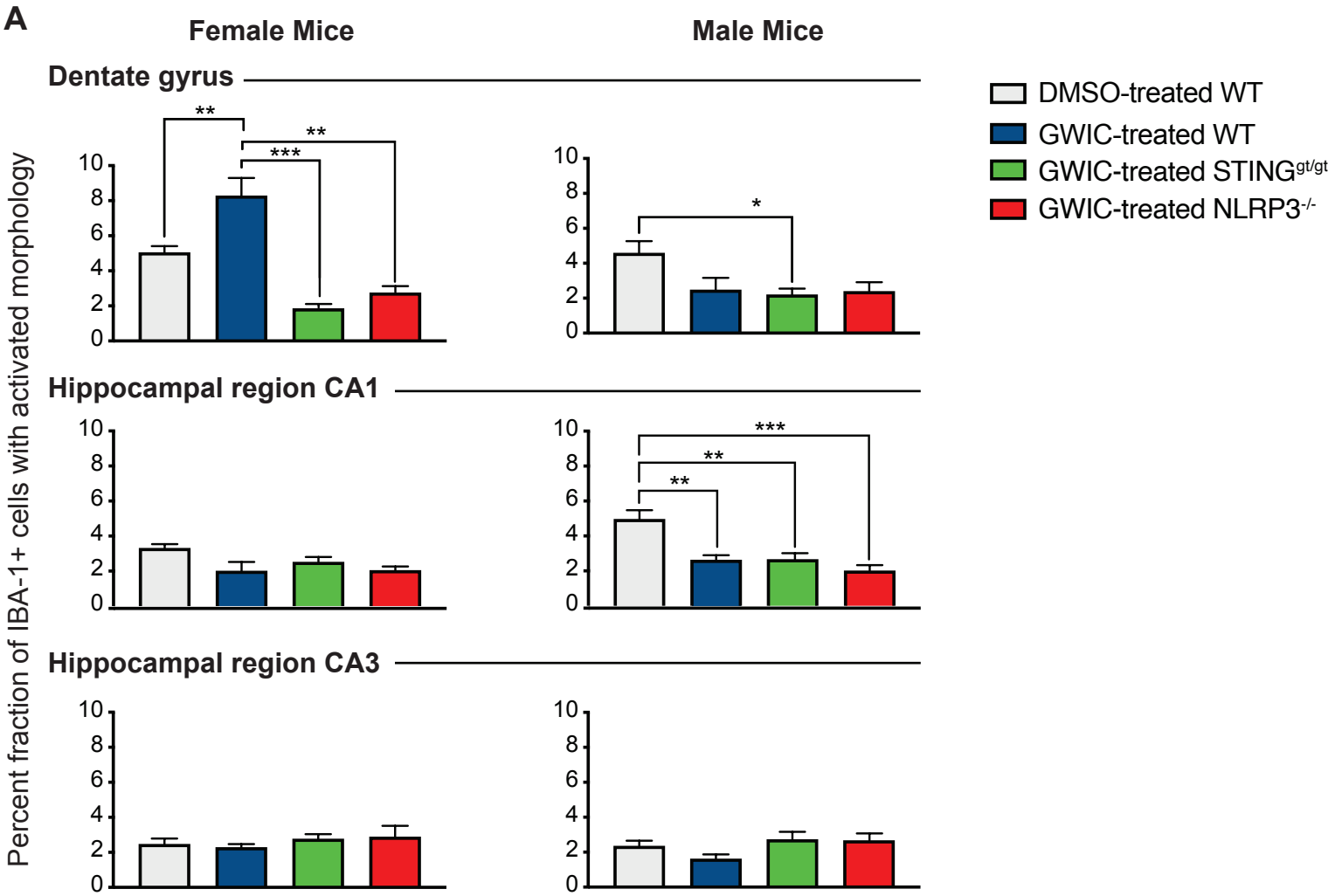

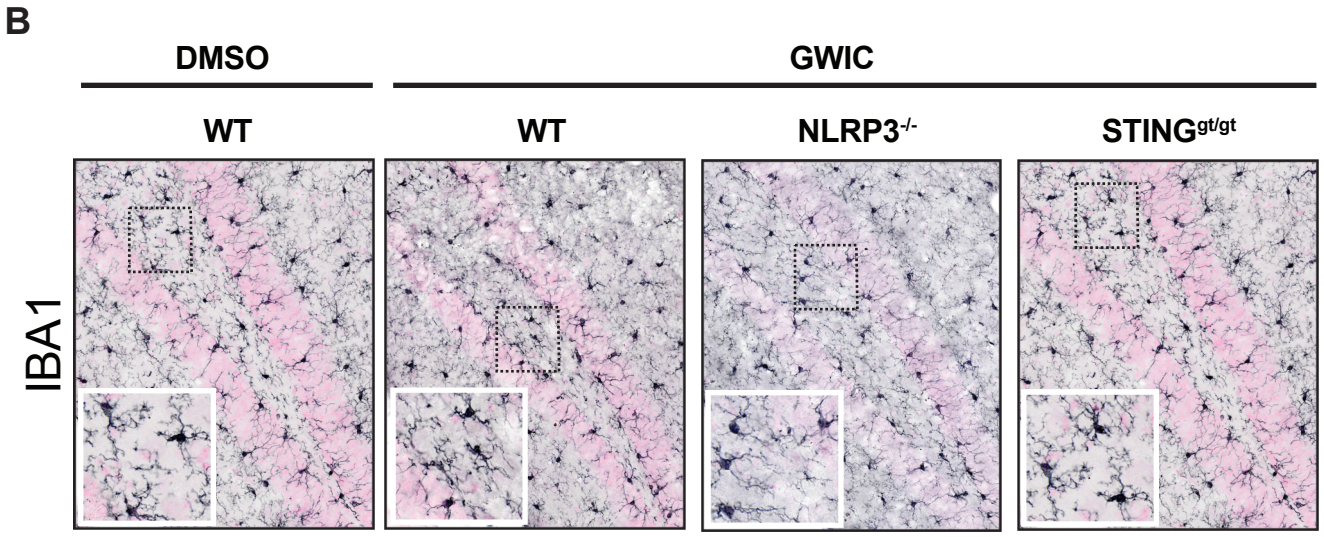

814 **Supplementary Figure 7. Analysis and imaging of IBA-1+ cells in the hippocampi of WT,**
815 **NLRP3$^{-/-}$ and STING$^{gt/gt}$ mice. (A)** Quantification of percent IBA-1+ cells with activated
816 morphology in three hippocampal regions (DG, CA1, and CA3) in DMSO- and GWIC-exposed
817 WT and GWIC-exposed NLRP3$^{-/-}$ and STING$^{gt/gt}$ female and male mice. Sections were scored
818 blindly for total number of IBA-1+ cells and number of IBA-1+ cells with activated morphology.
819 Error bars represent the mean of biological replicates +/- SEM (n=6). Indicated p-values were
820 calculated using two-tailed, unpaired, Student's t-test. *$p < 0.05$; **$p < 0.01$; **** $p < 0.0001$.
821 Absence of statistical information indicates a lack of statistical significance. (B) Images show
822 representative distribution and morphology of IBA-1+ microglia in the DG region of female
823 DMSO- and GWIC-exposed WT, and GWIC-exposed NLRP3$^{-/-}$ and STING$^{gt/gt}$ mice (scale bar =
824 100 μM). Insets show magnified views (scale bar = 50 μM).

825 **References**

826 1. Golomb, B. A. Acetylcholinesterase inhibitors and Gulf War illnesses. *Proc. Natl. Acad. Sci.*
827 *U. S. A.* **105**, 4295–4300 (2008).
828 2. White, R. F. *et al.* Recent research on Gulf War illness and other health problems in veterans of
829 the 1991 Gulf War: Effects of toxicant exposures during deployment. *Cortex J. Devoted Study*
830 *Nerv. Syst. Behav.* **74**, 449–475 (2016).
831 3. Shetty, G. A. *et al.* Chronic Oxidative Stress, Mitochondrial Dysfunction, Nrf2 Activation and
832 Inflammation in the Hippocampus Accompany Heightened Systemic Inflammation and
833 Oxidative Stress in an Animal Model of Gulf War Illness. *Front. Mol. Neurosci.* **10**, (2017).
834 4. Koslik, H. J., Hamilton, G. & Golomb, B. A. Mitochondrial dysfunction in Gulf War illness
835 revealed by 31Phosphorus Magnetic Resonance Spectroscopy: a case-control study. *PloS One*
836 **9**, e92887 (2014).
837 5. Golomb, B. A. *et al.* Coenzyme Q10 benefits symptoms in Gulf War veterans: results of a
838 randomized double-blind study. *Neural Comput.* **26**, 2594–2651 (2014).
839 6. Chen, Y. *et al.* Role of mitochondrial DNA damage and dysfunction in veterans with Gulf War
840 Illness. *PLOS ONE* **12**, e0184832 (2017).
841 7. Abdullah, L. *et al.* Translational potential of long-term decreases in mitochondrial lipids in a
842 mouse model of Gulf War Illness. *Toxicology* **372**, 22–33 (2016).
843 8. Emmerich, T. *et al.* Phospholipid profiling of plasma from GW veterans and rodent models to
844 identify potential biomarkers of Gulf War Illness. *PLOS ONE* **12**, e0176634 (2017).
845 9. Zakirova, Z. *et al.* Complementary proteomic approaches reveal mitochondrial dysfunction,
846 immune and inflammatory dysregulation in a mouse model of Gulf War Illness. *PROTEOMICS*
847 *– Clin. Appl.* **11**, 1600190 (2017).

848 10. Castro-Marrero, J. *et al.* Could mitochondrial dysfunction be a differentiating marker
849 between chronic fatigue syndrome and fibromyalgia? *Antioxid. Redox Signal.* **19**, 1855–1860
850 (2013).
851 11. Zhang, Q. *et al.* Changes in immune parameters seen in Gulf War veterans but not in
852 civilians with chronic fatigue syndrome. *Clin. Diagn. Lab. Immunol.* **6**, 6–13 (1999).
853 12. Johnson, G. J., Slater, B. C. S., Leis, L. A., Rector, T. S. & Bach, R. R. Blood Biomarkers
854 of Chronic Inflammation in Gulf War Illness. *PloS One* **11**, e0157855 (2016).
855 13. Parkitny, L., Middleton, S., Baker, K. & Younger, J. Evidence for abnormal cytokine
856 expression in Gulf War Illness: A preliminary analysis of daily immune monitoring data. *BMC*
857 *Immunol.* **16**, 57 (2015).
858 14. Broderick, G. *et al.* A pilot study of immune network remodeling under challenge in Gulf
859 War Illness. *Brain. Behav. Immun.* **25**, 302–313 (2011).
860 15. Broderick, G. *et al.* Altered immune pathway activity under exercise challenge in Gulf War
861 Illness: an exploratory analysis. *Brain. Behav. Immun.* **28**, 159–169 (2013).
862 16. Janulewicz, P. A. *et al.* The Gut-Microbiome in Gulf War Veterans: A Preliminary Report.
863 *Int. J. Environ. Res. Public. Health* **16**, (2019).
864 17. Craddock, T. J. A. *et al.* Using gene expression signatures to identify novel treatment
865 strategies in gulf war illness. *BMC Med. Genomics* **8**, 36 (2015).
866 18. Seth, R. K. *et al.* Gut DNA Virome Diversity and Its Association with Host Bacteria
867 Regulate Inflammatory Phenotype and Neuronal Immunotoxicity in Experimental Gulf War
868 Illness. *Viruses* **11**, (2019).
869 19. West, A. P. Mitochondrial dysfunction as a trigger of innate immune responses and
870 inflammation. *Toxicology* **391**, 54–63 (2017).

871 20. West, A. P., Shadel, G. S. & Ghosh, S. Mitochondria in innate immune responses. *Nat.*
872 *Rev. Immunol.* **11**, 389–402 (2011).
873 21. Nakahira, K., Hisata, S. & Choi, A. M. K. The Roles of Mitochondrial Damage-Associated
874 Molecular Patterns in Diseases. *Antioxid Redox Signal* **23**, 1329–1350 (2015).
875 22. Ojo, J. O. *et al.* Exposure to an organophosphate pesticide, individually or in combination
876 with other Gulf War agents, impairs synaptic integrity and neuronal differentiation, and is
877 accompanied by subtle microvascular injury in a mouse model of Gulf War agent exposure.
878 *Neuropathol. Off. J. Jpn. Soc. Neuropathol.* **34**, 109–127 (2014).
879 23. Zakirova, Z. *et al.* A Chronic Longitudinal Characterization of Neurobehavioral and
880 Neuropathological Cognitive Impairment in a Mouse Model of Gulf War Agent Exposure.
881 *Front. Integr. Neurosci.* **9**, 71 (2015).
882 24. Zakirova, Z. *et al.* Gulf War agent exposure causes impairment of long-term memory
883 formation and neuropathological changes in a mouse model of Gulf War Illness. *PLoS ONE* **10**,
884 0119579 (2015).
885 25. Heboyan, V. *et al.* Sex Differences in Gulf War Illness: A Reanalysis of Data From the
886 CDC Air Force Study Using CDC and Modified Kansas Case Definitions. *J. Occup. Environ.*
887 *Med.* **61**, 610–616 (2019).
888 26. Fernández-Arjona, M. D. M., Grondona, J. M., Granados-Durán, P., Fernández-Llebrez,
889 P. & López-Ávalos, M. D. Microglia Morphological Categorization in a Rat Model of
890 Neuroinflammation by Hierarchical Cluster and Principal Components Analysis. *Front. Cell.*
891 *Neurosci.* **11**, 235 (2017).

892 27. Hattiangady, B. *et al.* Object location and object recognition memory impairments,
893 motivation deficits and depression in a model of Gulf War illness. *Front. Behav. Neurosci.* **8**,
894 78 (2014).
895 28. Parihar, V. K., Hattiangady, B., Shuai, B. & Shetty, A. K. Mood and memory deficits in a
896 model of Gulf War illness are linked with reduced neurogenesis, partial neuron loss, and mild
897 inflammation in the hippocampus. *Neuropsychopharmacol. Off. Publ. Am. Coll.*
898 *Neuropsychopharmacol.* **38**, 2348–2362 (2013).
899 29. Zakirova, Z. *et al.* A Chronic Longitudinal Characterization of Neurobehavioral and
900 Neuropathological Cognitive Impairment in a Mouse Model of Gulf War Agent Exposure.
901 *Front. Integr. Neurosci.* **9**, 71 (2015).
902 30. Kelly, B. & O'Neill, L. A. Metabolic reprogramming in macrophages and dendritic cells
903 in innate immunity. *Cell Res.* **25**, 771–784 (2015).
904 31. Alhasson, F. *et al.* Altered gut microbiome in a mouse model of Gulf War Illness causes
905 neuroinflammation and intestinal injury via leaky gut and TLR4 activation. *PLoS ONE* **12**,
906 (2017).
907 32. Gao, D. *et al.* Cyclic GMP-AMP Synthase is an Innate Immune Sensor of HIV and Other
908 Retroviruses. *Science* **341**, (2013).
909 33. Chen, Q., Sun, L. & Chen, Z. J. Regulation and function of the cGAS-STING pathway of
910 cytosolic DNA sensing. *Nat Immunol* **17**, 1142–1149 (2016).
911 34. Elliott, E. I. & Sutterwala, F. S. Initiation and perpetuation of NLRP3 inflammasome
912 activation and assembly. *Immunol Rev* **265**, 35–52 (2015).
913 35. Man, S. M. & Kanneganti, T.-D. Converging roles of caspases in inflammasome activation,
914 cell death and innate immunity. *Nat Rev Immunol* **16**, 7–21 (2016).

915 36. Sauer, J.-D. *et al.* The N-ethyl-N-nitrosourea-induced Goldenticket mouse mutant reveals
916 an essential function of Sting in the in vivo interferon response to Listeria monocytogenes and
917 cyclic dinucleotides. *Infect. Immun.* **79**, 688–694 (2011).
918 37. Kovarova, M. *et al.* NLRP1-dependent pyroptosis leads to acute lung injury and morbidity
919 in mice. *J. Immunol. Baltim. Md 1950* **189**, 2006–2016 (2012).
920 38. Abdullah, L. *et al.* Lipidomic profiling of phosphocholine-containing brain lipids in mice
921 with sensorimotor deficits and anxiety-like features after exposure to Gulf War agents.
922 *Neuromolecular Med.* **14**, 349–361 (2012).
923 39. Joshi, U. *et al.* Oleoylethanolamide treatment reduces neurobehavioral deficits and brain
924 pathology in a mouse model of Gulf War Illness. *Sci. Rep.* **8**, 12921 (2018).
925 40. Joshi, U. *et al.* Targeting sirtuin activity with nicotinamide riboside reduces
926 neuroinflammation in a GWI mouse model. *Neurotoxicology* **79**, 84–94 (2020).
927 41. Abdullah, L. *et al.* Proteomic CNS profile of delayed cognitive impairment in mice
928 exposed to Gulf War agents. *Neuromolecular Med.* **13**, 275–288 (2011).
929 42. Kodali, M. *et al.* Curcumin treatment leads to better cognitive and mood function in a
930 model of Gulf War Illness with enhanced neurogenesis, and alleviation of inflammation and
931 mitochondrial dysfunction in the hippocampus. *Brain. Behav. Immun.* **69**, 499–514 (2018).
932 43. Madhu, L. N. *et al.* Neuroinflammation in Gulf War Illness is linked with HMGB1 and
933 complement activation, which can be discerned from brain-derived extracellular vesicles in the
934 blood. *Brain. Behav. Immun.* **81**, 430–443 (2019).
935 44. Shetty, A. K. *et al.* Monosodium luminol reinstates redox homeostasis, improves cognition,
936 mood and neurogenesis, and alleviates neuro- and systemic inflammation in a model of Gulf
937 War Illness. *Redox Biol.* **28**, 101389 (2020).

938 45. Patten, E. & Parker, K. Women in the U.S. Military: Growing Share, Distinctive Profile.
939 6.
940 46. Zundel, C. G. *et al.* Rates of Chronic Medical Conditions in 1991 Gulf War Veterans
941 Compared to the General Population. *Int. J. Environ. Res. Public. Health* **16**, (2019).
942 47. Pierce, P. F. Federal Nursing Service AwardMonitoring the Health of Persian Gulf War
943 Veteran Women. *Mil. Med.* **170**, 349–354 (2005).
944 48. Coughlin, S. S. *et al.* A Review of Epidemiologic Studies of the Health of Gulf War
945 Women Veterans. *J. Environ. Health Sci.* **3**, 0–0 (2017).
946 49. Koslik, H. J., Hamilton, G. & Golomb, B. A. Mitochondrial Dysfunction in Gulf War
947 Illness Revealed by 31Phosphorus Magnetic Resonance Spectroscopy: A Case-Control Study.
948 *PLOS ONE* **9**, e92887 (2014).
949 50. Chen, Y. *et al.* Role of mitochondrial DNA damage and dysfunction in veterans with Gulf
950 War Illness. *PLoS ONE* **12**, (2017).
951 51. Zakirova, Z. *et al.* Complementary proteomic approaches reveal mitochondrial
952 dysfunction, immune and inflammatory dysregulation in a mouse model of Gulf War Illness.
953 *Proteomics Clin. Appl.* **11**, (2017).
954 52. Butterick, T. A. *et al.* Gulf War Illness-associated increases in blood levels of interleukin
955 6 and C-reactive protein: biomarker evidence of inflammation. *BMC Res. Notes* **12**, (2019).
956 53. Carpenter, J. M. *et al.* Neurochemical and neuroinflammatory perturbations in two Gulf
957 War Illness models: Modulation by the immunotherapeutic LNFPIII. *NeuroToxicology* **77**, 40–
958 50 (2020).

959 54. Parkitny, L., Middleton, S., Baker, K. & Younger, J. Evidence for abnormal cytokine
960 expression in Gulf War Illness: A preliminary analysis of daily immune monitoring data. *BMC*
961 *Immunol* **16**, 57 (2015).
962 55. Golomb, B. A. *et al.* Coenzyme Q10 Benefits Symptoms in Gulf War Veterans: Results of
963 a Randomized Double-Blind Study. *Neural Comput.* **26**, 2594–2651 (2014).
964 56. Holodniy, M. & Kaiser, J. D. Treatment for Gulf War Illness (GWI) with KPAX002
965 (methylphenidate hydrochloride + GWI nutrient formula) in subjects meeting the Kansas case
966 definition: A prospective, open-label trial. *J. Psychiatr. Res.* **118**, 14–20 (2019).
967